

Vibration dissipation in a surgical microscope support system

N.F. de Wit

Technische Universiteit Delft

Vibration dissipation in a surgical microscope support system

by

N.F. de Wit

to obtain the degree of Master of Science
at the Delft University of Technology,
Faculty Mechanical, Maritime and Materials Engineering,
at the Department Biomechanical Engineering,
to be defended on 17 October 2017 at 14:00.

Student number: 4086090
Project duration: September 1, 2016 – October 1, 2017
Thesis committee: Prof. dr. J. Dankelman, BMD, TU Delft
dr. P. Lambert, PME, TU Delft
Ass. Prof. G. Smit, BMD, TU Delft
ir. L. van Bommel, Hittech Multin

This thesis is confidential and cannot be made public until October 2022.

An electronic version of this thesis is available at <http://repository.tudelft.nl/>.



Abstract

A surgical microscope is a stereo, optical device that is positioned near the patient to magnify, illuminate and record the working area during surgery. The different types of surgical procedures, the variety of tools used by the surgeon and the varying viewpoint of the surgeon combined, makes it a very dynamic situation where the microscope should fit in. (Re)positioning the microscope on different locations and under different angles is therefore essential. The support system of the microscope should allow for manual, effortless and fluent repositioning to make it extremely user-friendly. Activation of the brakes in all the joints turns the flexible system into a rigid one.

In this rigid mode the support system should be a steady base for the microscope, but certain support systems currently on the market cannot realize this. The microscope keeps vibrating in its eigenmode for too long after a perturbation from its equilibrium position, which causes a deteriorated image. A quicker return to the equilibrium position allows the surgeon to continue the operation without much delay. An investigation in the design of a steady but repositionable support system for a surgical microscope is therefore desired.

The strategy used in this thesis to improve the design of the system is by creating a dynamic simulated model of the microscope support system in order to perform a free vibration analysis. The model has been validated with vibration measurements performed on an actual system. To investigate possible improvements of the vibration response, the model has been subjected to a set of parametric experiments. A second strategy to improve the vibration response is by implementing a subsystem with damping properties: A tuned mass damper.

The results of the parametric experiments show that the settling time of the support system can be reduced with 17.5% by slight adjustments to certain design variables. These results have been transformed into design recommendations. The tuned mass damper has successfully been implemented in the simulated model of the support system. This subsystem has great damping properties: The addition of a tuned mass damper shows that the settling time can be reduced with 77.4%.

When a tuned mass damper is implemented in the support system of a surgical microscope, delays after microscope repositioning actions will significantly be reduced which shortens the total operation time. Verification of these results in practice are left for future work.

Acknowledgements

I would like to thank several people who helped me through this graduation project. To the persons that were closest to the project, Jenny Dankelman, Patrice Lambert and Leonard van Bommel: Thanks for the guidance, the helpful meetings and the comments on the report.

The company Hittech Multin was an excellent place to carry out this project: A good working area and nice colleagues with whom I had refreshing lunchbreak walks. In my opinion, the company would fit in the ideal image of a working area for mechanical engineers. I would also like to thank Felix Bischoff and Wolfgang Robra from Hittech Prontor for their help with my measurements and their time for spending dinner with me.

Further thanks goes: To Rogier Polak from Flow engineering for the kind welcome at their company, the long and informative conversation about tuned mass dampers and the tour through the workplace. To Chris Verheul from Sayfield International for having a Skype-meeting about my Adams model. To Radboud Koot from the Leids Universitair Medisch Centrum for allowing me to attend a surgery and answering my questions about the surgical microscope.

Last but not least I would like to thank my family, friends and my girlfriend for their interest in the project and their support for keeping me motivated.

Contents

1	Introduction	7
1.1	Problem statement	9
1.2	Current surgical microscope support systems	10
1.3	Prior art	11
1.4	Research goal	12
1.5	Thesis outline	12
2	Simulated model	15
2.1	Three-dimensional modelling with MSC Adams software	15
2.1.1	Model subdivision	15
2.1.2	Initial configurations	17
2.1.3	Design variables	18
2.1.4	Parametric analysis methods	19
2.1.5	Optimization objectives	19
2.1.6	Constraints	20
2.1.7	Simulation script	20
2.2	Dynamic performance of the initial system	21
3	Model validation	23
3.1	Experimental determination of the system parameters	23
3.1.1	Static equalization	25
3.1.2	Dynamic validation	26
3.2	Two dimensional modelling of basic links	27
4	Parametric analysis	29
4.1	Modelling experiments and results	30
4.1.1	Parametric analysis of the lengths of the links.	31
4.1.2	Parametric analysis of the masses	33
4.1.3	Parametric analysis of the torsion stiffnesses	37
4.1.4	Parametric analysis of the torsion damping variables	40
4.1.5	Parametric analysis of the link inertias	42
4.1.6	Parametric analysis of the relative position of the CoM	44
4.2	Multiple system configurations	45
4.2.1	Other direction of applied force	47
4.3	Valid parameter range in practice	48
4.4	Combined maximum improvement	49

5	Tuned mass damper	51
5.1	Tuned mass damper design	52
5.1.1	Equivalent single-degree-of-freedom system	52
5.1.2	Den Hartog method: optimal TMD design	53
5.1.3	TMD placement	54
5.1.4	Den Hartog method in practice	55
5.2	Simulated microscope support system model and the tuned mass damper	55
5.2.1	Model of the tuned mass damper	57
6	Discussion and conclusion	61
6.1	Comparison of two different improvement methods	61
6.2	Modelling consequences: Errors due to simplifications	62
6.3	Future work	63
6.4	Conclusion	63
7	Appendices	65

1

Introduction

When the limit of the naked eye has been reached a surgical microscope proves its value in surgery. A surgical microscope is an optical device that is positioned above the patient to enhance the view on the working area by creating a magnified and enlightened image. The working area is an open wound, often deep and difficult to reach. Perfect alignment of the microscope to the wound is essential to not obstruct the light for vision.

In figure 1.1 a commonly used surgical microscope is displayed on the right. The light path from the wound to the surgeons eyes runs through the objective lens, then via a set of lenses and prisms and finally through the oculars. The surgeon is able to look at the working area with a magnification between 4x and 40x[4]. The surgeon has depth perception of the working area because a three dimensional image is made with a stereo lens orientation (created with two identical light paths through the microscope)[5]. The working distance of these microscopes is large, 150-700mm[7], because the surgeon must fit with his hands between the objective lens and the working area. As can be seen, multiple sets of binoculars can be installed on the microscope enabling assistants of the surgeon a view on the working area as well. The modularity of the microscope results in the fact that the total mass is adjusted, which is an important aspect for the weight balancing of these systems.

The support system has the function to keep the microscope in position and provide a base for other features. The type of support system focussed on in this project consists of a mobile heavy foot and a serial manipulator arm with rotational joints at the locations displayed in figure 1.2a. The support system is designed to position and balance the end-effector (the microscope) with all six degrees-of-freedom over a range displayed in figure 1.2b.

The vertical motion of the microscope is realized with a parallelogram between point B and point C in figure 1.2a. The weight balancing implies gravity compensation[6] of the microscope by a subsystem (e.g. counterweight, spring) in the support system. (Re)positioning the microscope inside a certain volume exactly where the surgeon wants is an important factor due to the dynamic environment in the operation room. The

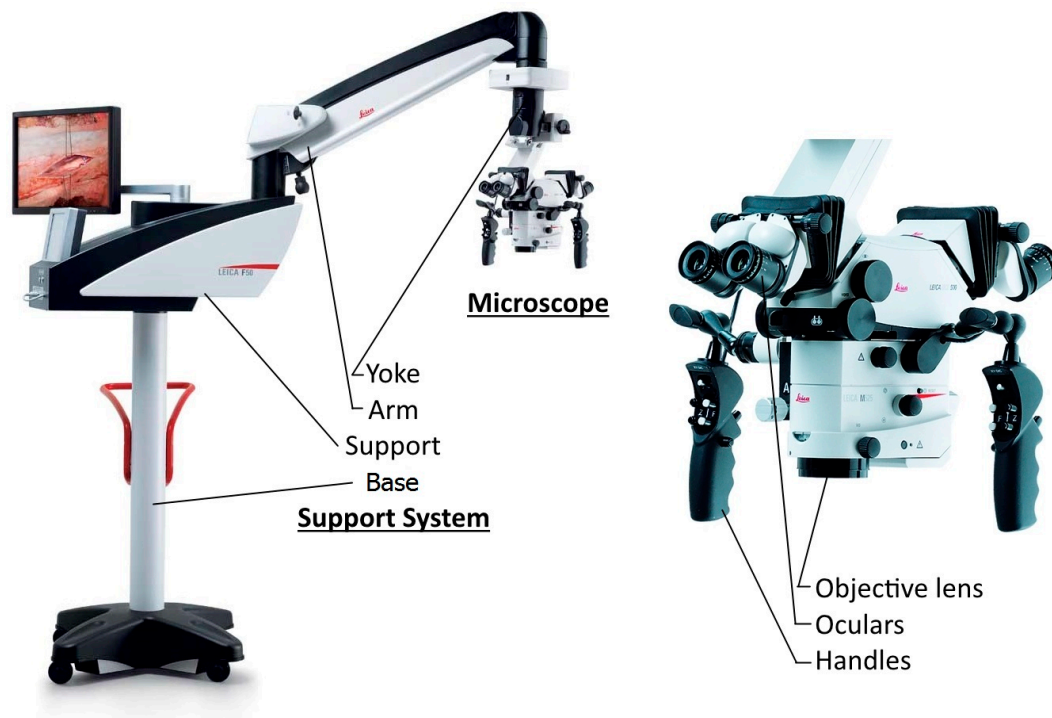


Figure 1.1: A mobile surgical microscope system for procedures in Neurosurgery, Spine, Otolaryngology, and Plastic Reconstructive surgery[2].

repositioning is performed multiple times per operation, so to make it extremely user-friendly this should be effortless and fluent. The repositioning is executed manually by the surgeon via one handle or both handles on the sides of the microscope. When pressing brake-buttons on these handles the brakes in each joint are disabled and the system is able to be moved, when releasing them the system becomes rigid again.

After preparation of the wound and initialization of the microscope, the system is ready to be wheeled towards the patient by the non-sterile assistant. Subsequently, the surgeon or the sterile assistant are able to move the microscope close to the wound. During the surgical procedure mainly small distance repositioning takes place, while the surgeon uninterruptedly looks through the microscope. At an observational study at the LUMC during a Microvascular Decompression (open brain surgery), it was noted that the microscope was actively used for two hours. In the two hours, the microscope was being repositioned for over 20 times. A repositioning action was found to consist of the following 8 steps:

1. Free hand or both hands from instrument(s)
2. Grab microscope handle(s) purely by touch or combined with making visual contact
3. Push brake button(s) to release the brakes in each joint
4. Apply manual force to move the microscope into the new desired position
5. Release brake button(s)
6. Adjust magnification, focus point or light intensity if necessary

7. Release handle(s)
8. Move hand(s) back to instrument and grab it by touch or by making visual contact too

This repositioning action must not be confused with zooming, focusing or lighting actions. For these actions the brakes do not need to be released and moreover, with many systems, there are foot- and mouth-control options. Assistants in the operation room are also able to perform these actions on the touch-screen (see figure 1.1) by listening to instructions given by the surgeon. Lastly, new systems often have the feature of auto-focus techniques. In the book by Jabbour[8] it is stated that surgeons may spend up to 40% of their total time in surgery making adjustments to the microscope. This very high percentage must include zooming, focusing and adjusting the light as well. Whether this has been a good estimate or not, the adjustments to a surgical microscope take up a large part of the operation time.

1.1 Problem statement

When the microscope is positioned at the exact location the surgeon has planned and the image is clear, the brake-buttons are released and the hands can be taken of the handles (Step 7 of the repositioning action). This action causes a perturbation from the actual equilibrium position of the system, which results in a vibrating microscope and therewith a deteriorated image. One can visualize this with the situation when one wants to put a hanging lamp in its stable equilibrium position with his/her hands. Even with great effort the lamp often swings slightly after releasing the lamp. Other sources of vibration are building vibrations and collisions between personnel and the support system. Building vibrations only occur in a few cases when the building itself is not robust enough and collisions are rare incidents.

As mentioned, the surgeon spends a large share of the operation time on adjustments to the microscope, so it is undesired that each time an extra delay is present: The surgeon should not have to wait for the vibrations to damp out after every repositioning action. The support system shakes in its natural frequency and returns to its equilibrium position after a certain amount of time due to the systems natural damping. The 2%-settling time of such a system is about six and a half seconds (section 3.1.2). The vibrating rigid support system can be imagined as a cantilever beam perturbed from its equilibrium position that slowly transforms the energy in the system into heat.

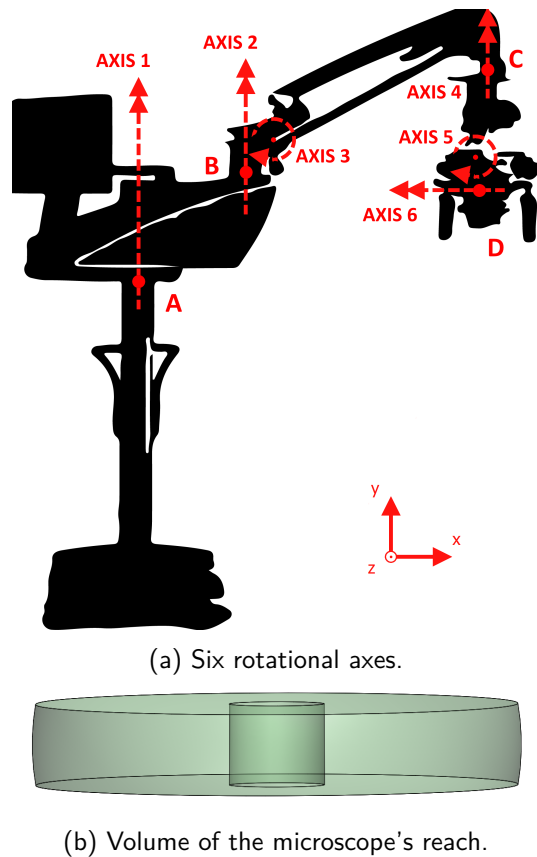


Figure 1.2: Mobility of the support system.

The source of the vibrations can hardly be eliminated from the environment, because the surgeon simply has to grab and release the microscope to reposition it. The support system itself, that vibrates in its natural frequency, needs further study to resolve the problem. Therefore, the problem that will be treated in this project can be stated as follows:

A surgical microscope that vibrates due to insufficient stability of the support system results in a deteriorated image which lengthens the total operation time of a surgical procedure.

1.2 Current surgical microscope support systems

In figure 1.3, from left to right, it is shown that the surgical microscope can be mounted on[1]

- Table top stand
- Ceiling or wall system
- Surgeon's head
- Portable floor stand(1.3b and 1.3c)

Floor stands are the most common support systems for surgical microscopes[3]. There are two types of floor stand surgical microscope support systems: One with the SCARA principle and vertical balancing(figure 1.3b) and one with a double balancing mechanism (figure 1.3c). The double balancing mechanism makes this type even more expensive. This project will focus on the SCARA/single balancing type of support system, because with these systems the vibrations persevered the longest.



(a) Table top mount[20], Ceiling or wall mount[22] and Head mount[19].

(b) Floor stand: SCARA and single balancing[21].

(c) Floor stand: double balancing[21].

Figure 1.3: Different types of surgical microscope support systems.

1.3 Prior art

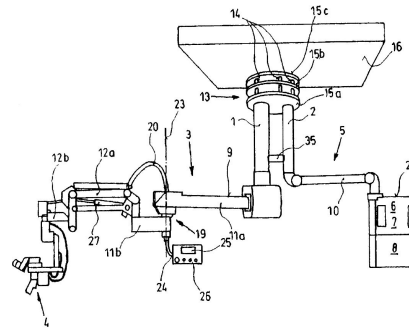
Research in the field of reducing the vibrations in support systems of surgical microscopes is scarce. The production of stable support systems is performed by manufacturers that do not publish their findings in literature. Though, patents have been found that claim to have designed ceiling mounts with higher stability: A decoupled mount (figure 1.4a) and a delta-arm mount (figure 1.4a).

A general trend in the design of support systems is a strive for increasing stiffness. Stiff systems deflect less than compliant systems with equal applied forces, but do have a higher natural frequency.

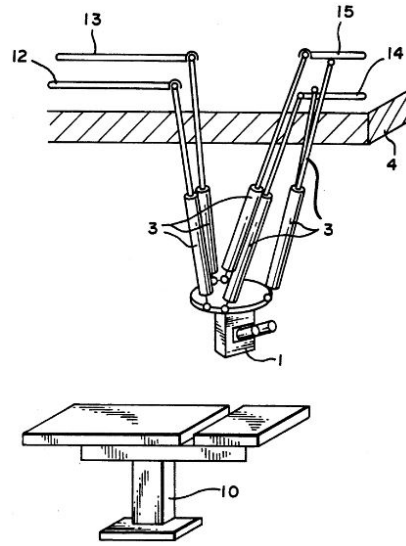
A complete different approach to improve the image of the working area is by using a digital microscope decoupled from the visualising module: The image is recorded by a light sensitive chip and directly projected on a monitor. The chip is much lighter than the current device and it is therefore possible to use a different design for the support of this digital microscope. The surgeon still perceives a three-dimensional image with the right monitor-glasses combination [11].

A Dutch engineering company reduced vibrations in a surgical microscope by implementation of an intermediate system between the ceiling and the system that actively damps external vibrations [12]. Sensors in the active vibration isolation platform (so-called Hummingbird platform, figure 1.4c) detect low-frequent vibrations in the ceiling and counteract them with actuators.

There were no studies found that the microscope support system itself was subjected to a parametric analysis to improved the dynamic response. Also, studies focussed on the assumption that the source of the vibrations is the building and not the user itself. Therefore it is justifiable that this research should be performed.



(a) Decoupling of the system [9].



(b) Delta ceiling suspension with a high static and dynamic stability [10].



(c) Microscope mounted to the Hummingbird vibration isolation platform [12].

Figure 1.4: Vibration dissipation strategies for surgical microscope support systems

1.4 Research goal

The main objective of this master thesis is formulated as follows:

Reduce the settling time of the surgical microscope support system with 20%.

The project focusses on the floor stand SCARA support system. A 2%-settling time is used to have a quantitative measure and is calculated with equation 1.4.1.

$$t_s = \frac{-\ln\left(0.02\sqrt{1-\zeta^2}\right)}{\zeta\omega_n} \quad (1.4.1)$$

ω_n in [rad/s] represents the first natural frequency of the system and ζ is the unit-less damping ratio. The settling time of the original and new system will be compared. The reduction of 20% is chosen as a realistic but challenging guess: If the settling time of a system is 5 seconds and it can be improved in such a way that it settles in 4 seconds, the reduction can be calculated with equation 1.4.2.

$$\left(\frac{4-5}{5}\right) 100\% = -20\% \quad (1.4.2)$$

The research question of this master thesis is formulated as follows:

In which ways must the design of the support system be adapted to reduce its settling time without downgrading the functionality of the support system?

"Functionality of the system" implies the long list of aspects and requirements the system needs to meet. A list of the most important aspects is given below:

- Robustness: A stiff structure
- Ease of repositioning: Low friction in the joints
- Slender structure: Sufficient clearance around the microscope
- Perfect balancing: Releasing the brakes cannot result in a sudden motion

1.5 Thesis outline

For engineers it is helpful to understand the performance of a system early in the design or analysis process. However, it is impractical to test a large set of physical parameter adaptations directly on such a system to understand its behaviour after a disturbance. Therefore, a simulated model of the surgical microscope support system can offer a solution. The performance of the model is representative for the performance of the actual system.

In figure 1.5 a schematic overview of this research process is displayed. Via the virtual world (right) an attempt is made to improve a system in the real world (left). The top right block is treated in chapter 2 and explains the simulated model of the microscope support system. Chapter 3 will discuss the experiments performed on an existing system (upper left block) which are used to validate the model (middle right block). Experiments with parameter adaptations can be performed on the model and provide

the user with a different behaviour as a result of the adaptations. The quantitative term of the behaviour, the measure how well the system performs, helps to select the adaptations that improve the system the most. The lower right block represents these experiments and results and this is discussed in chapter 4. Chapter 5 treats a side project that runs parallel to the main project and has the same goal. In this section it is discussed how well the dynamic behaviour of the support system improves, when a novel subsystem is added. Finally, recommendations to improve the dynamic response of the system (lower left block) are discussed in chapter 6.

With this strategy, the simulated model helps to reach the objective of this thesis project stated in section 1.4. The decision making for the design of the actual system can be influenced by the findings from a simulation of the model.

To my knowledge, the surgical microscope support system has not yet been subjected to a simulated dynamic analysis. Therefore, this project can provide important insight in the system.

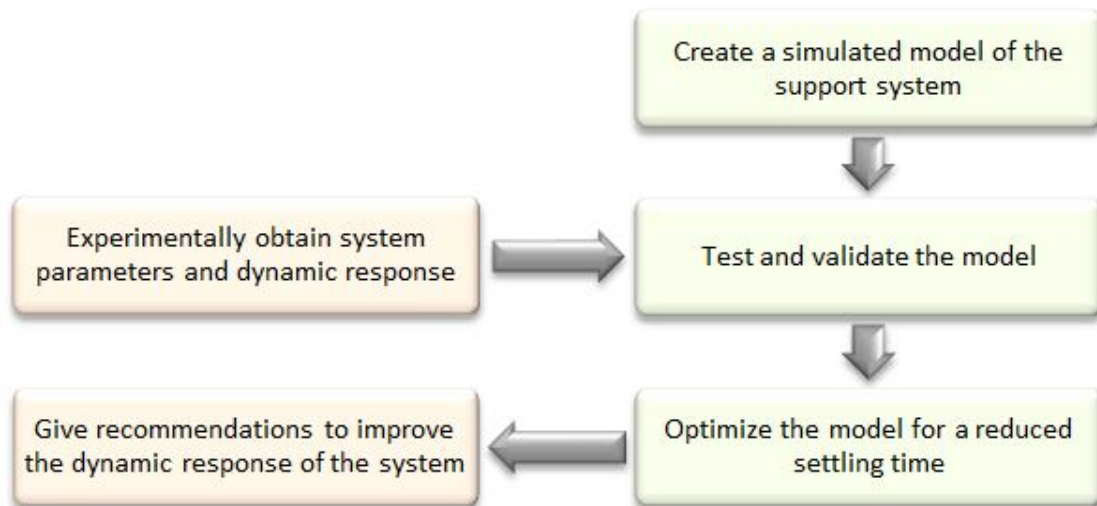


Figure 1.5: Block diagram of the outline with left the real world and right the virtual world.

This research project has been executed in cooperation with the company Hittech. This company designs the Arm and Yoke for certain microscope support systems.

2

Simulated model

In this section, an explanation will be given of the model that is used to provide answers to the research question. The adaptable simulated model for principle design considerations is a tool for reaching the goal of the project.

Major adaptations to the support system can quickly be investigated using a simulated model of the surgical microscope support system. Performing such investigations on an actual device is highly impractical due to fabrication and experimental time and costs. In section 4 these investigations in the form of experiments will be discussed.

The effort for generating a simulated model pays off when a large set of different positions of the support system need to be analysed. The complexity of the microscope support system has been described in the introduction.

2.1 Three-dimensional modelling with MSC Adams software

The surgical microscope support system is a complex three dimensional structure that should be modelled in three dimensions as well to properly investigate its behaviour.

MSC Adams is worldwide the most used multibody dynamics software. This software has been used to simulate a model of a microscope support system, because the software is also able to let you efficiently improve the model design with parametric analysis tools. These tools help with the investigation of the influence of design variables on model performance.

2.1.1 Model subdivision

The model of the microscope support system exists of five bodies: four rigid links and an end mass, see figure 2.1. The four links are named Base, Support, Arm, Yoke respectively from ground to microscope and are coloured from dark to light blue (Similar to the names in figure 1.1). The end mass represents the microscope itself and is coloured

yellow. The amount of bodies was found to be the best consideration between: Having enough bodies to describe the system in a sufficient manner and keeping the number of bodies low to stay away from overcomplicating the model calculations.

The links are interconnected with spherical joints. In these joints, the three translations are constraint and the three rotations are counteracted by three independent torsional stiffnesses. Independent damping variables are added as well in these joints.

The system has a total of six axis which allow the microscope to be able to be positioned in six degrees of freedom. A video with each rotation animated will be shown during the thesis presentation. The model has an equal amount of joints that can be pre-set to mimic each position of the system.

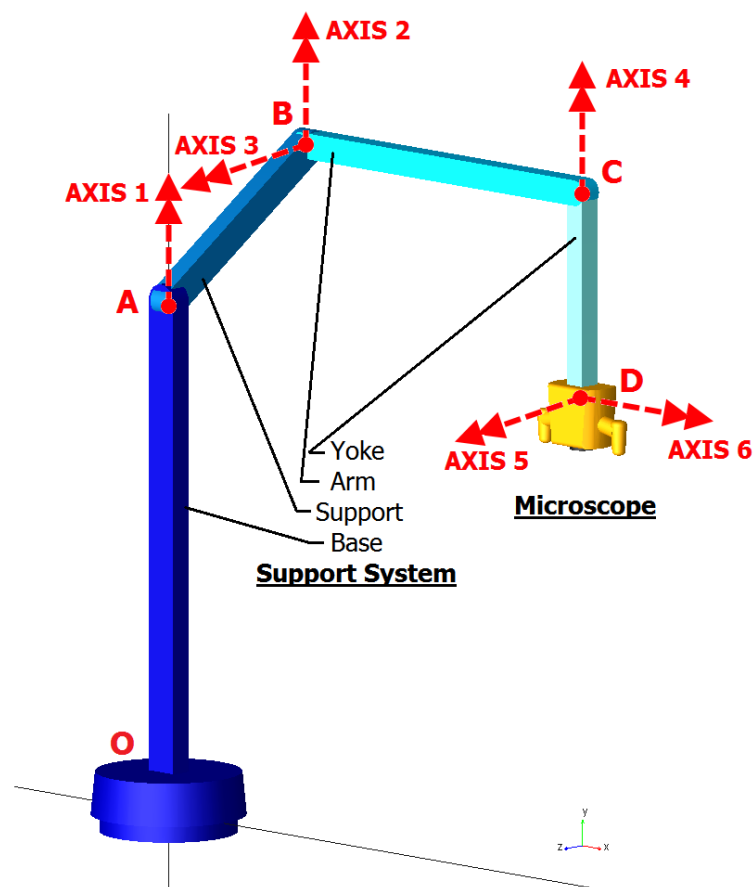


Figure 2.1: Virtual model of the support system, configuration nr. 1 (see table 2.1).

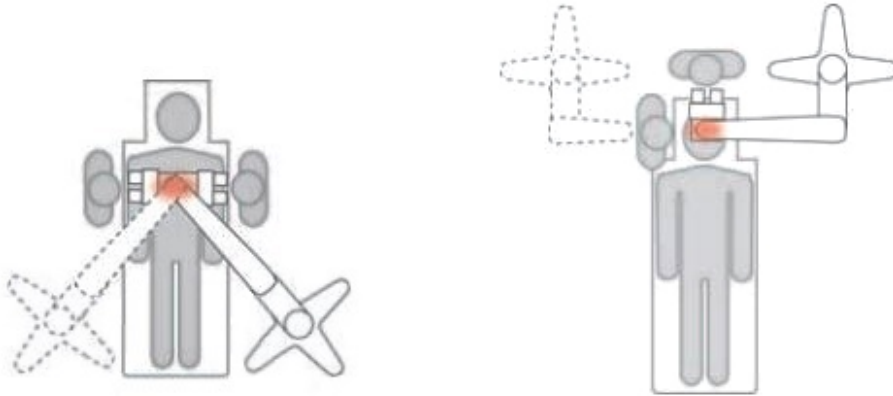
2.1.2 Initial configurations

The configuration of the support system can be adjusted with three angles in order to place the microscope at a certain location in space. Axis one and two allow the microscope to be positioned in the horizontal plane in an annulus. Axis three allows the microscope to be positioned in the vertical direction. The combination results in a sphere-section as the reach of the microscope (figure 1.2b).

Table 2.1: Six support system configurations.

Nr.	Configuration axis 1 and 2 [degrees]	Configuration axis 3 [degrees]
1	90	0
2	90	+20
3	90	-20
4	0	0
5	0	+20
6	0	-20

Six important configurations where axis 1,2 and 3 are varied as stated in table 2.1 will be treated in this report. Figure 2.2 shows the top-view of respectively configuration



(a) Straight system configuration.

(b) 90 degree system configuration.

Figure 2.2: Two basic system configurations[2].

4 and 1: the "straight" and "90 degree" system configuration. The orientation of the Arm is horizontal. The Yoke is always perpendicular to the vertical axis due to the parallelogram in the Arm. The two configurations displayed in the figure are the common ones in operations.

Initial deflection

The dynamical vibrations are generated when a constant force at the end point is gently applied and suddenly removed, creating an oscillation around its equilibrium position. The force needs to be applied gently because this prevents initial noise. The applied force over time of equation 2.1.1 is displayed in figure 2.3. The gravity in the simulation has been turned off to prevent an initial oscillation in the vertical direction when the

simulation is started. This is valid because it is a constant force field applied to every part of the system.

$$F_j [\text{STEP}(\text{time}, 0, 1, 4, 0) - \text{STEP}(\text{time}, 5, 1, 5.01, 0)] \quad (2.1.1)$$

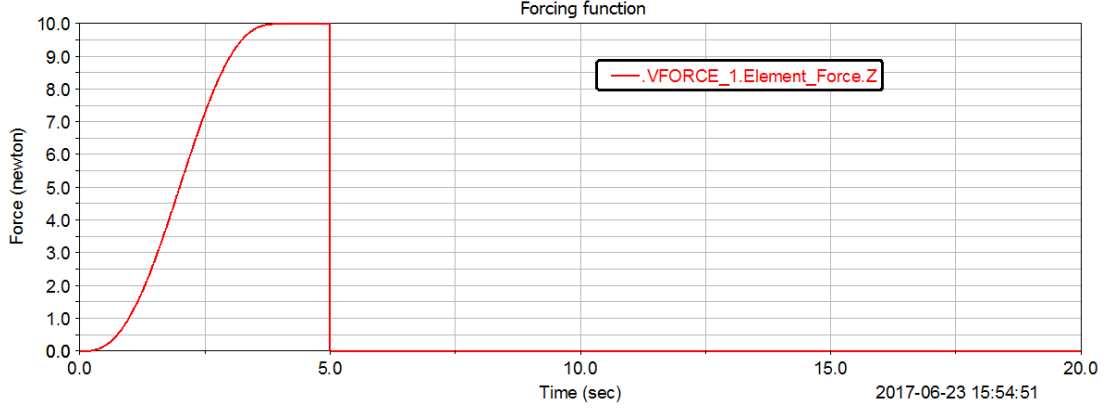


Figure 2.3: Force-time graph of the function that generates the initial displacement.

2.1.3 Design variables

All the independent parameters that influence the behaviour of the model are listed in table 2.2. The initial values of all these design variables are listed as well in the table. Each value is defined based on measurements performed on an actual system (The measurements are explained in section 3.1). Column one contains the 12 independent

Table 2.2: Design variables and their initial values.

Stiffness	$[\frac{Nm}{rad}]$	Damp- ing	$[\frac{Ns}{m}]$	Mass, Length, Force	$[kg],$ $[m],$ $[N]$	Inertia	$[kgm^2]$	Angles, CoM	$[rad],$ $[\%]$
TOx =	2.78E+05	zOx=	75	M1=	160	1-Ixx=	19	axis1=	$-\pi/2$
TOy =	5.55E+05	zOy=	85	M2=	20	1-Iyy=	4.3	axis2=	$-\pi/2$
TOz =	2.78E+05	zOz=	75	M3=	35	1-Izz=	19	axis3=	0
TAx =	9.25E+05	zAx=	75	M4=	7	2-Ixx=	0.5	axis4=	0
TAy =	5.55E+04	zAy=	85	Mmic=	10	2-Iyy=	0.12	axis5=	0
TAz =	3.15E+05	zAz=	75	L1=	1.20	2-Izz=	0.5	axis6=	0
TBx =	9.25E+03	zBx=	85	L2=	0.55	3-Ixx=	0.5	CoM1=	20%
TBy =	2.59E+04	zBy=	80	L3=	0.90	3-Iyy=	2.37	CoM2=	50%
TBz =	3.52E+04	zBz=	80	L4=	0.45	3-Izz=	2.37	CoM3=	50%
TCx =	9.25E+03	zCx=	80	Fx=	0	4-Ixx=	0.2	CoM4=	50%
TCy =	2.41E+04	zCy=	75	Fy=	0	4-Iyy=	0.05		
TCz =	3.88E+04	zCz=	80	Fz=	-10	4-Izz=	0.2		
						Imic=	0.1		

torsional stiffnesses in the the four spherical joints and the second column contains the 12 independent torsional damping variables. The Third column contains the five masses, the four lengths of the the links and the values of the constant term in the applied force.

The fourth column contains the 13 mass moments of inertia. The fifth column contains the initial angles between the links and the position of the centre of mass along the link in percentage. Each variable requires a predefined range which forces a design study to keep the variable within these particular limits. Ultimately, parametric analyses can automatically modify (a set of) design variables to improve the model.

2.1.4 Parametric analysis methods

During a parametric analysis, the influence of each design variable is investigated based on the quantitative value of the model performance. This will be fully covered in chapter 4. Adams runs a series of simulations in which design variables are being modified and the effect is provided as feedback in the form of the objective (section 2.1.5). There are three investigation methods:

- Design study: Investigate the effect of varying one design variable. The design variable is being varied within its preset range and the effect on the microscope dynamics can be viewed.
- Design of Experiments (DoE): Investigate the effect of varying several design variables simultaneously. Same for a design study but now with more variables at once.
- Optimization: Adjusts design variables to minimize or maximize a preset objective. The design variables are adjusted in such a way that the objective is best met. Overall constraints can be added as well to search for an objective within certain boundaries.

2.1.5 Optimization objectives

The settling time has already been mentioned as a quantitative measure for judgement on the performance. However, this measure is not suited as an optimization objective because it is a relative value and with the used software, it was not possible to construct an optimization objective with the settling time. Therefore, a new quantitative measure is created.

It is common knowledge that the area under the velocity-time curve is equal to the displacement. When an objective is chosen that minimizes this area, the microscope covers less distance. Less distance in a certain time interval means less image deterioration. The area can be approached by computing the Riemann sum. A Riemann sum approximates the computation of an integral by a finite sum of the heights in a function. This method is used because the software does not have an option for a real integral computation.

In equation 2.1.2 the total displacement S is obtained from the absolute value of the velocity of the microscope v , the total modelling time t_{end} and the time step t_{step} . The function $LAST_N(_, _)$ makes sure that only the oscillating part is calculated, so from 5 seconds till 20 seconds. This objective is called a measure of performance. During the parametric analysis, the software minimizes the objective to create a quantitative value of the objective which is used for distinguishing improvements and worsening.

$$S = \frac{\text{SUM}(\text{LAST}_N(\text{ABS}([v_{microscope}]) * t_{end}, \frac{3}{4} * t_{end} * t_{step}))}{(\frac{3}{4} * t_{end} * t_{step})} \quad (2.1.2)$$

2.1.6 Constraints

An overall constraint should be added to the optimization if the design variables are allowed to vary between their limits, but an overall design variable must be respected. Three constraints that will be investigated are discussed here.

The total weight of the system can not exceed a certain value:

$$M_1 + M_2 + M_3 + M_4 + M_{mic} < C_M \quad (2.1.3)$$

The endpoint, the microscope, must stay at the same location. This means that the overall length cannot change, but individual link lengths can be interchanged:

$$L_{h,tot} = L_{2,x} + L_{3,x} == C_{L,x} \quad (2.1.4)$$

$$L_{v,tot} = L_{1,y} + L_{2,y} + L_{3,y} + L_{4,y} == C_{L,y} \quad (2.1.5)$$

2.1.7 Simulation script

A script is used to perform a simulation, without having to pre-set the preferences every time. The total simulation time t_{end} is equal to 20 seconds and the time step t_{step} is equal to 0.02. A smaller step size improves the accuracy of the simulation, but makes it slower too. Another option to tune the numerical solver is by adjusting the dynamic and kinematic acceptable error. The time step and each tolerance are chosen as follows: First the acceptable errors are set really small (range of 1E-010) and the performance of the system is calculated with the model objective. Then, the errors are increased factor 10 step by step up till the moment that the performance starts to differ. At that point the tolerances are small enough to give an accurate result and large enough for fast simulations.

2.2 Dynamic performance of the initial system

The model of the microscope support system with the initial values from table 2.2 is simulated with the simulation script. The applied forcing function lets this model vibrate in its eigenfrequencies and the damping coefficients in the joints let the model return to the equilibrium position. The most important output of the model is the system response: The displacement-time curve in the direction of the applied force as shown in figure 2.4.

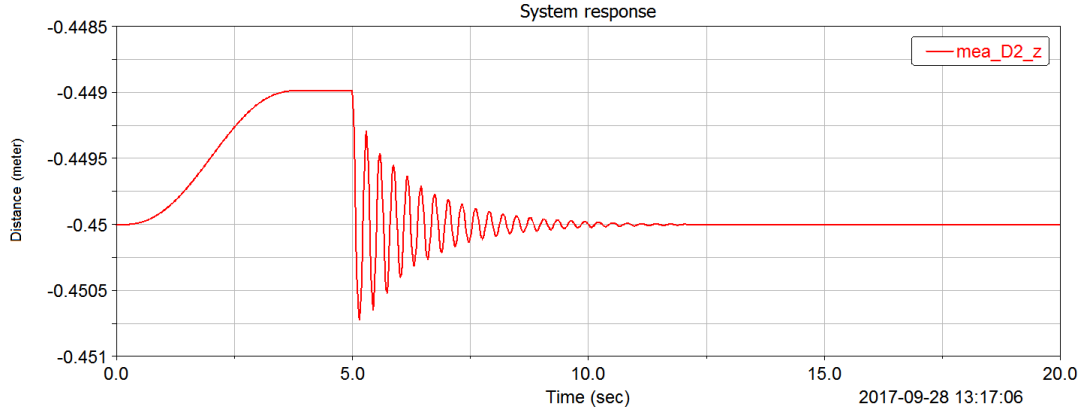


Figure 2.4: Measure on the displacement of the microscope in z-direction over time, configuration nr. 1. Equilibrium position is in z-direction 0.45 meter from the x-axis.

For this configuration, it can be seen that a force of -10 N results in a static displacement of 1.02 mm and the vibrations are more or less dissipated after 5 seconds. The quantitative value of the performance of this system is $S = 21.45$ mm, calculated with equation 2.1.2.

The software can compute the linear modes and animate them each individually. The output of such a computation with the twelve eigenmodes is listed below. The first eigenmode is the vibration of the microscope in z-direction with a frequency of 3.45 Hz. The second mode shows an oscillation in vertical y-direction. Higher modes show more complex deflections including torsions. Counting the number of peaks in a certain time spectrum of figure 2.4 results in a frequency equal to 3.45 Hz. The damping factor for this mode is 3.6%. The videos of these modes will be shown during the thesis presentation.

MODE NUMBER	UNDAMPED NATURAL FREQUENCY (Hz)	DAMPING RATIO	REAL	IMAGINARY
1	3.454017E+00	3.597506E-02	-1.242585E-01 +/-	3.451781E+00
2	4.928621E+00	1.865222E-02	-9.192973E-02 +/-	4.927763E+00
3	6.065227E+00	3.930622E-02	-2.384012E-01 +/-	6.060540E+00
4	7.430770E+00	9.601367E-02	-7.134555E-01 +/-	7.396440E+00
5	1.187185E+01	1.337962E-01	-1.588408E+00 +/-	1.176511E+01
6	3.193346E+01	8.877438E-01	-2.834874E+01 +/-	1.470018E+01
7	1.005781E+02	9.853833E-01	-9.910798E+01 +/-	1.713366E+01
8	2.048420E+01	1.254563E-01	-2.569872E+00 +/-	2.032236E+01
9	3.117987E+01	1.597078E-01	-4.979667E+00 +/-	3.077966E+01
10	6.017986E+01	5.845261E-02	-3.517670E+00 +/-	6.007696E+01

11	8.458900E+01	5.057350E-02	-4.277962E+00	+/-	8.448075E+01
12	2.356487E+02	4.405589E-01	-1.038171E+02	+/-	2.115474E+02

The natural frequency in configuration nr. 4 is smaller, namely 3.01 Hz. The graph in figure 2.5 shows indeed a slightly larger period. The static displacement is 1.22 mm and the damping ratio is 2.6%. This "straight" configuration is clearly a more troublesome initial position because the static deflection is higher and the dynamic oscillations persist longer. This configuration has therefore been used as starting point for the experiments described in chapter 4.

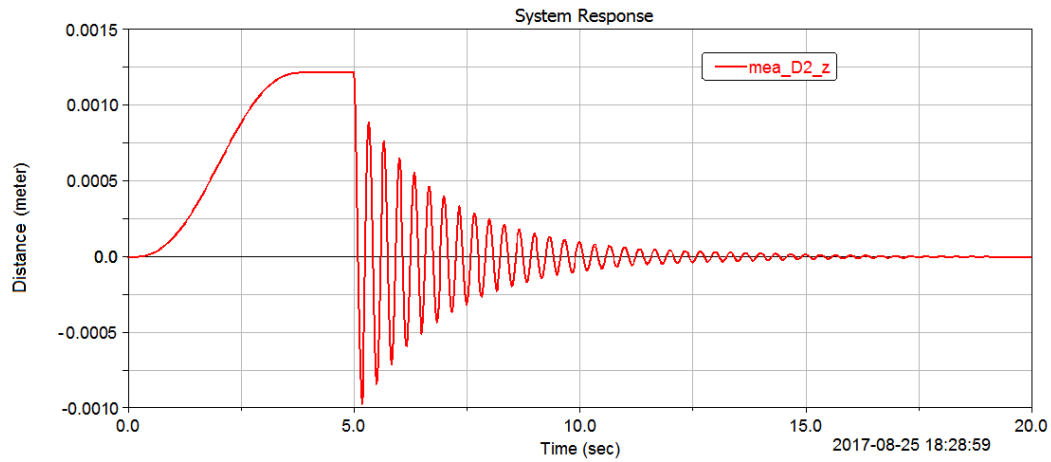


Figure 2.5: Measure on the displacement of the microscope in z-direction over time, configuration nr. 4.

3

Model validation

The created model of the microscope support system needs to be validated to check if it is a proper representation of the actual system. The three-dimensional Adams model is a sufficient model for representing the actual system for the research that is performed in this thesis project, because the outcome of the model is similar to the outcome of an experimental system identification of an actual system. These measurements are further explained in section 3.1.

The validation process can be divided into two parts: The static equalisation and dynamic validation. The first one deals with matching the static properties of the model to the static properties of the actual system. The second one deals with checking whether the results from the dynamic model match the results from the experiments executed on a actual system.

3.1 Experimental determination of the system parameters

An actual SCARA microscope support system available for vibration measurements was not present at Hittech Multin. Its sister company, Hittech Prontor in Calmbach (Germany), had one suitable system in their building that already had been used for experiments, so it was decided that the measurements should be executed there. One and a half day were enough to subject this system to a large set of experiments and there was even time left to perform some equivalent experiments on a different system (pictures in Appendix C).

The goal of the experiments was to understand the vibrational response of the system after a perturbation from the equilibrium position. The perturbations were applied at the microscope in three orthogonal directions and the system was positioned in six different configuration (see table 4.12). This resulted in a huge list of data such that nothing would be missed, because a second moment for experiments was not possible. The data was neatly organised: The name of the data file contained the type of experiment, the system configuration, the direction of the applied force, the direction of measurement and the time and date.

The data was generated by a laser displacement sensor (for its properties see Appendix D) and processed with Labview (for its block diagram see Appendix B). Although this sensor only measures distance in one direction, it was preferred to be used for oscillation measurements over a 3D-acceleration sensor, because the acceleration sensor had a lower resolution. The resolution of the laser was $3.1 \mu\text{m}$ which has been calculated as follows:

- The laser was able to measure the distance to a surface between 22,5 mm and 27,5 mm so it has a range of 5 mm.
- The output voltage was ranged in a linear way between 2 and 10 Volt.
- A 12 bit National Instrument data acquisition (NI-DAQmx) was able to process 2000 bits between 0 and 10 Volt
- Therefore, between 2 and 10 volt a number of $0.8 * 2000 = 1600$ bits could be processed
- The resolution is $5 \text{ mm}/1600 \approx 0.0031 \text{ mm}$

A stable manoeuvrable stand with easy fastening screws was used to position the displacement sensor at a distance of 25 mm from the surface of the microscope. The sensor was not only positioned at location D (the microscope, figure 1.2a), but also at location A, B and C. Also, the orientation of the sensor was varied in three orthogonal directions. The forces were applied with a Correx force gauge. The output of Labview was each time an Excel file and these files were further processed with Matlab. An example graph of the raw data from one experiment is displayed in figure 3.1.

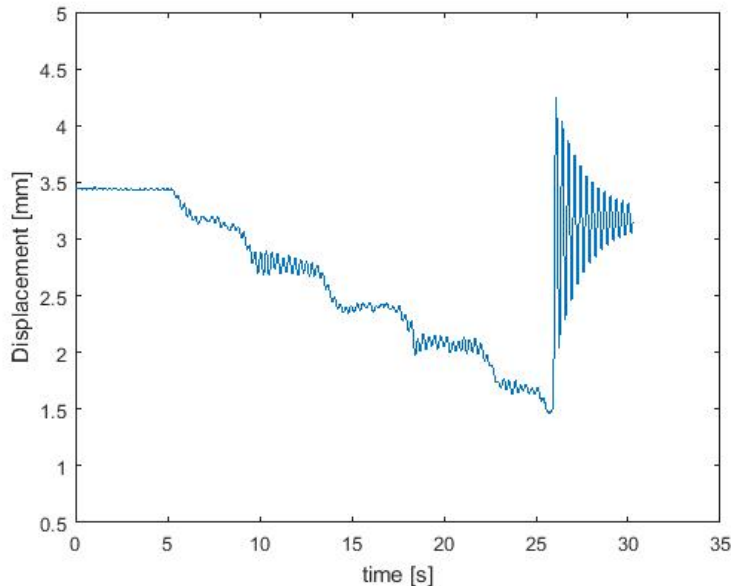


Figure 3.1: Deflection measurement from equilibrium position of point C in z-direction, Configuration 4, force applied in z-direction.

With this gathered data, Matlab was used to obtain the stiffness, eigenfrequency and damping coefficient of each link in every system configuration. The stiffness was calculated from dividing the applied force with the measured displacement from the equilibrium position. The dimensions of the support system were simply measured with a

tape-measure between points A till D. The widths don't have an effect on the model, because the mass moments of inertia will be used as parameters that take the mass distribution along the length of the link into account.

The masses of the sections were more difficult to obtain. Disassembling the complete system to weigh each section was not an option. CAD files of the system and similar systems were used to obtain these numbers. Additional benefit of these CAD files was the possibility to calculate the moments of inertia as well.

3.1.1 Static equalization

The static force applied to the surgical microscope generated a displacement from its equilibrium position that should be the same as the virtual displacement from the equilibrium position of the model with an equal applied virtual force, in all three directions.

The measured deflections of configuration nr. 4 at the joints (table 3.1) are used to calculate the deflections at the centre of mass of each link (First column of table 3.2).

Table 3.1: Measured static deflection in z-direction for a force $F_z = -10\text{N}$.

Point	Deflection [mm]
A	0.09
B	0.50
C	1.69
D	2.64

Table 3.2: Static CoM deflection from the measurements and from the model in z-direction for a force $F_z = -10\text{N}$.

Point	Measured deflection [mm]	Modelled deflection [mm]
CoM Base	0.02	0.01
CoM Support	0.39	0.12
CoM Arm	1.09	0.45
CoM Yoke	2.16	0.94
CoM Microscope	2.63	1.22

The results show that the deflections of the CoM's in the measurements are about two to three times higher than the displacements of the CoM's in the model (Second column of table 3.2). An explanation for this error can be a systematic measuring error because the backlash (or play) was not taken into account: The direction of the applied force in relation to the direction of the laser measurement.

The play of the surgical microscope has not been investigated. In hindsight, this would have been an interesting subject for investigation because then the reliability of the measurements would have been higher.

3.1.2 Dynamic validation

Due to the large amount of data, it was necessary to efficiently process it. A Matlab script (Appendix E) was made that performed actions such as selecting useful data, normalization of the data and plotting a suitable fit over the peaks of the oscillations. Also, a fast Fourier transform was calculated to produce a single-sided frequency spectrum of the vibration response. From the frequency spectrum, the first eigenfrequency can be obtained and in some cases also the second and third.

It was found that for the system in configuration 4, the average eigenfrequency of the first mode was equal to 3.08 Hz. Comparing this with the frequency of the model in the same configuration shows a good match: 3.01 Hz in table 4.12.

Even the second and third eigenfrequencies from the frequency spectrum match good with the modelled ones: Respectively 4.45 Hz, 6.50 Hz, 4.43 Hz and 6.96 Hz. Adams is able to animate the mode of each eigenfrequency. The animation of the second mode shows an oscillation of the microscope in vertical direction. The measurements also show a domination of the 4.45 Hz when the force is applied in vertical direction and when the laser displacement sensor is orientated in vertical direction. The measured average eigenfrequency in the 90 degree, horizontal configuration is 3.35 Hz and the modelled one is 3.45 Hz. The damping coefficients from the measurements ranged for different system configurations between the 2.5% and 6.2%. It was found that the model damping coefficients ranged between the 2.1% and 5.3%.

With this information, the average settling time of the actual system and the model can be compared. Equation 1.4.1 gives an average settling time of 6.69 seconds. The average settling time of the modelled system is with 6.42 seconds quite similar.

Another remarkable resemblance deals with the direction of the applied force. During the measurements, it was noticed that the vibrations in z-direction were often dominant, even though the force was applied in x- or y-direction. The same behaviour was found with the virtual model as explained in section 4.2.1.

3.2 Two dimensional modelling of basic links

Before the experiments in Germany were going to be executed, vibration measurements were performed on an Arm test module at Hittech Multin to get familiar with the measuring equipment. A picture of the Arm test module, called the FUMU, is displayed in figure 3.2 and the raw displacement data is displayed in figure 3.3. The same experimental procedure was followed as explained earlier in this chapter. An overview of the results obtained from the FUMU is given in table 3.3. These results are compared with three modelling methods: Analytically with basic mechanical calculations, with a numerical solver in Matlab and with a simulation in Adams.



Figure 3.2: Test set-up for the Arm module. Stand for the sensor in lower left corner.

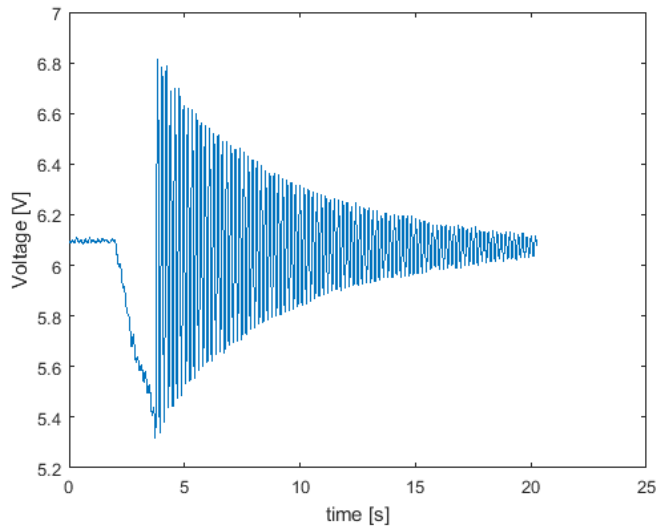


Figure 3.3: Raw measurement data of the deflection of the FUMU.

The eigenfrequencies obtained from these three modelling methods were almost the same as from the measurements on the FUMU. Equation 3.2.1 shows how to analytically determine the eigenfrequency of an equivalent undamped system. This expression can be derived from basic mechanical formulas, as is explained at the website of brown.edu[13]. In Hertz this results in $f_n = 5.35$ Hz.

Table 3.3: FUMU parameters obtained from the measurements.

M_{end}	26.8 kg
m_{arm}	1.5 kg
L	0.70 m
k_{transl}	31250 N/m
k_{rot}	15312 Nm/rad
f_n	5.35 Hz
ζ	0.54%

$$\omega_n = \sqrt{\frac{k_{trans} * L - m_{arm} * g/2 - M_{end} * g}{m_{arm} * L/3 + M_{end} * L}} \quad [rad/s] \quad (3.2.1)$$

Modelling a link in Matlab can be done as follows: Create a moment equilibrium of a link with the Newton-Euler method, build an equation of motion (equation 3.2.2) and numerically integrate it with the ODE45 solver.

$$\ddot{\theta} = \frac{-(c\dot{\theta}) + T_{tot}}{J_{tot}} \quad (3.2.2)$$

The obtained eigenfrequency and damping coefficient were 3.35 Hz and 0.55%.

Lastly, the link was modelled in Adams. The results after simulation are displayed below.

MODE NUMBER	UNDAMPED NATURAL FREQUENCY (Hz)	DAMPING RATIO	REAL	IMAGINARY
1	5.358616E+00	5.387244E-03	-2.886817E-02 +/-	5.358538E+00

These matching results are a stimulus for continuing with modelling of the microscope support system. Matlab was the preferred software for modelling because of the gathered experience with it over the years. However, The calculation time for a three dimensional, four link system appeared to be too long, even with making smart use of the TMT method. Adams software turned out to be a good alternative with a short simulation time, but with fewer analysing methods.

In a Skype meeting with Chris Verheul, an experienced Adams user working for the company Sayfield International, the model has been discussed. This was a good opportunity to ask questions about unclear functions in Adams en he was able to give some recommendations to make the model more robust.

4

Parametric analysis

The model described in chapter 2 exists of 59 design variables that influence the behaviour (See table 4.1, a copy of table 2.2). Investigation of this large set of variables is made manageable by defining several separate experiments.

Table 4.1: Design variables and their initial values.

Stiffness $[\frac{Nm}{rad}]$	Damp- ing $[\frac{Ns}{m}]$	Mass, Length, [kg], Force [N]	Inertia [kgm ²]	Angles, [rad], CoM [%]
TOx = 2.78E+05	zOx= 75	M1= 160	1-Ixx= 19	axis1= $-\pi/2$
TOy = 5.55E+05	zOy= 85	M2= 20	1-Iyy= 4.3	axis2= $-\pi/2$
TOz = 2.78E+05	zOz= 75	M3= 35	1-Izz= 19	axis3= 0
TAx = 9.25E+05	zAx= 75	M4= 7	2-Ixx= 0.5	axis4= 0
TAy = 5.55E+04	zAy= 85	Mmic= 10	2-Iyy= 0.12	axis5= 0
TAz = 3.15E+05	zAz= 75	L1= 1.20	2-Izz= 0.5	axis6= 0
TBx = 9.25E+03	zBx= 85	L2= 0.55	3-Ixx= 0.5	CoM1= 20%
TBy = 2.59E+04	zBy= 80	L3= 0.90	3-Iyy= 2.37	CoM2= 50%
TBz = 3.52E+04	zBz= 80	L4= 0.45	3-Izz= 2.37	CoM3= 50%
TCx = 9.25E+03	zCx= 80	Fx= 0	4-Ixx= 0.2	CoM4= 50%
TCy = 2.41E+04	zCy= 75	Fy= 0	4-Iyy= 0.05	
TCz = 3.88E+04	zCz= 80	Fz= -10	4-Izz= 0.2	
			Imic= 0.1	

Effectively, not all variables from table 4.1 need to be investigated. A parametric analysis solely on the 44 variables in table 4.2 is sufficient, based on the following hypotheses:

- TOx and TOz are equal because of the symmetry of the Base. Same counts for the damping factors zOx and zOz and inertias 1-Ixx and 1-Izz.
- (2-Ixx and 2-Izz), (3-Iyy and 3-Izz), (4-Ixx and 4-Izz), are all set to be equal as well.

- F_x and F_y are zero because during the simulations, only an initial forcing function is applied in z-direction.
- All six axis variables are only modified when the initial position of the model is changed.

Table 4.2: Design variables for parametric analysis.

L1	M1	TO _x (TO _z)	zO _x (zO _z)	Link 1-I _{xx} (1-I _{zz})	CoM1
L2	M2	TO _y	zO _y	1-I _{yy}	CoM2
L3	M3				CoM3
L4	M4	TA _x	zA _x	Link 2-I _{xx} (2-I _{zz})	CoM4
	Mmic	TA _y	zA _y	2-I _{yy}	
		TA _z	zA _z		
		TB _x	zB _x	Link 3-I _{xx}	
		TB _y	zB _y	3-I _{yy} (3-I _{zz})	
		TB _z	zB _z		
		TC _x	zC _x	Link 4-I _{xx} (4-I _{zz})	
		TC _y	zC _y	4-I _{yy}	
		TC _z	zC _z	Imic	

Another strategy that is used to make the analysis more structured, is by grouping the design variables. In table 4.2 groups already have been made by giving them each an own column. In section 4.1 each column is treated separately and in section 4.4 the results from each separate experiment are combined. It does not mean that the combined result is also the overall best result possible. Other sets of initial values might give a lower minimum of the model objective. However, in this thesis the decision has been made to not investigate the coupling effects of all parameters via brute force. This would be too computer intensive since the model objective of every possible combination of the 44 parameters will be calculated. Moreover, not much insight in the behaviour of the model is gathered with such an approach.

4.1 Modelling experiments and results

Length and mass design variables (column one and two of table 4.2) are being investigated separately and in addition, combinations of these variables are made to not violate the requirements. The effect of design variables from column three, four and five are displayed in their graphs per joint or per link to show the relative effect better. For the same reason, the effect of the location of the CoM, column six, is also displayed in one graph.

To model the worst case scenario, the straight system configuration (figure 2.2a) is investigated most thoroughly. More configurations will be discussed in section 4.2 and when conclusions are drawn, the mean value of the performance of multiple configurations will be calculated to give a good averaged image. The model of the straight system configuration vibrates with a natural frequency of 3.01 Hz after a force $F_z = -10$ N is applied on and suddenly removed from the system. The total displacement in the initial, straight configuration is equal to $S = 37.15$ mm calculated with equation 2.1.2.

Each graph in this chapter that shows results of a parametric analysis has the model objective on its vertical axis: the total displacement S from equation 2.1.2. On the horizontal axis the design variable(s) is being varied within its range.

4.1.1 Parametric analysis of the lengths of the links.

Table 4.3: Initial lengths of the model of the microscope support system.

Length	[m]
Base	1.20
Support	0.55
Arm	0.90
Yoke	0.45

Investigate what effect each individual link length has on the response of the system. The range is percent-relative to value: A range of -20% and +20% for each length is used. Each time, five default levels have been calculated because this shows the trend well enough. With more default levels the curve would be smoother, but the calculation time will be longer. For the length analysis of the Yoke, nine default levels have been calculated because a trend was more difficult to spot.

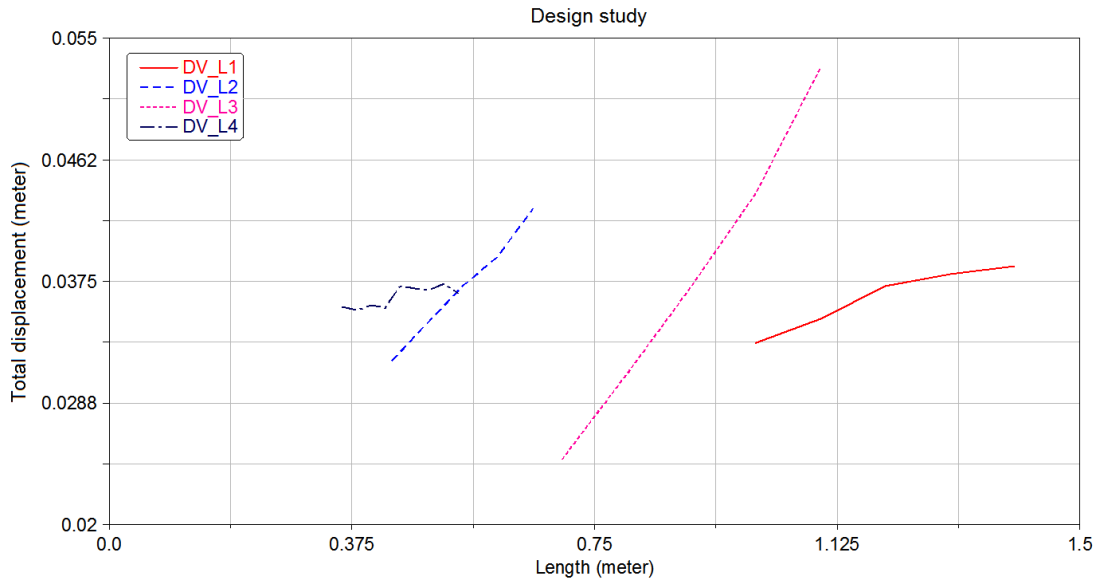


Figure 4.1: Results of the length analysis of the Base, Support, Arm and Yoke, configuration nr. 4. Link length on horizontal axis and performance measure on vertical axis.

Clearly the total displacement increases when the length of the Base, the Support and the Arm is increased. The effect is the greatest for adjustments of the length of the Arm. The total displacement does not show any correlation with altering the length of the Yoke.

Figure 4.2 shows that a similar effect is found for the microscope in configuration nr. 1.

The other experiments in this section will not treat the other configurations, but section 4.2 will.

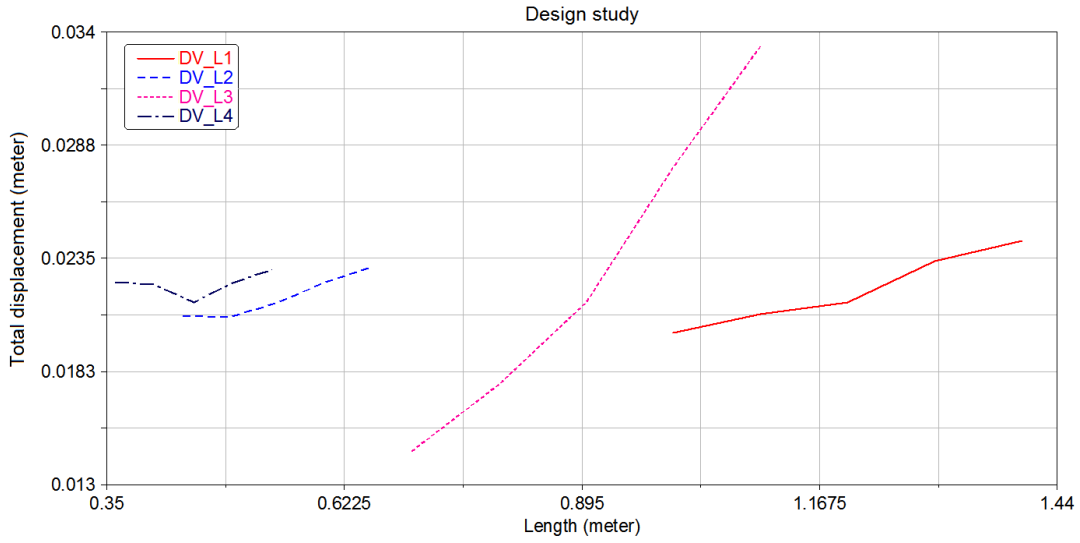


Figure 4.2: Results of the length analysis of the Base, Support, Arm and Yoke, configuration nr. 1. Link length on horizontal axis and performance measure on vertical axis.

From figure 4.1 it can be seen that when the system is being made smaller, the performance increases. The requirement that the microscope needs to be a certain distance from the base, addresses that link lengths cannot simply be decreased. However, in horizontal and vertical directions, the total length can be re-distributed. In configuration 4, the horizontal length of the Support $l_{s,x} = 0.5464 * \cos(0.6032) = 0.45$ m and the horizontal length of the Arm $l_{a,x} = 0.9$ m can be interchanged as long as the sum stays equal, as shown in table 4.4. For valid re-distribution of the length, an absolute-relative value is used instead of a percent-relative: The lengths will be increased or decreased with 0.10 meter. In total, 25 combinations are possible, but only 5 of them are valid and these are marked with an "x".

Table 4.4: Valid horizontal length re-distribution between the Support and the Arm.

		Support $l_{s,x}$ [m]				
		0.25	0.35	0.45	0.55	0.65
Arm $l_{a,x}$ [m]	0.7					x
	0.8				x	
	0.9			x		
	1.0		x			
	1.1	x				

Figure 4.3 shows the five valid length rearrangements in the horizontal way with the blue asterisks (Table 4.4 must be read column by column from top left to bottom right). In the figure, a slight trend can be spotted that when the Support length share is relatively larger than the share of the length of the Arm, the performance improves.

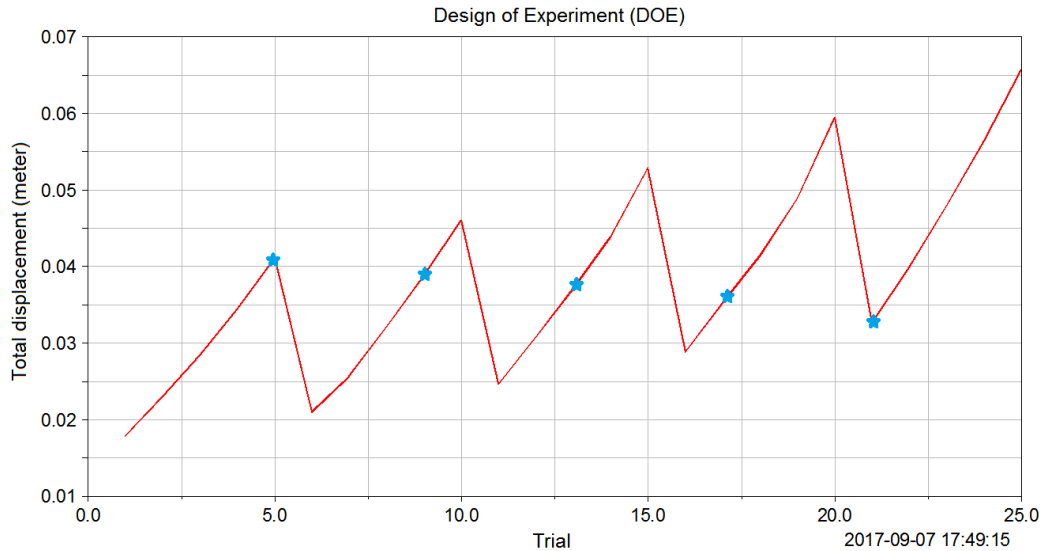


Figure 4.3: 25 possibilities of the horizontal length re-distribution between the Support and the Arm. The blue asterisks match with the "x"s in table 4.4. Combination trial on horizontal axis and performance measure on vertical axis.

The same will now be done in vertical direction. Working with the same configuration, the length in vertical direction of the Base is $l_{b,x} = 1.2$ m and the Support is $l_{s,x} = 0.5464 * \sin(0.6032) = 0.31$ m. The vertical length of the Yoke is being kept constant because the model objective was not affected by this design variable. Also, the clearance under the total arm becomes too small if the Yoke is shortened.

Table 4.5: Valid vertical length re-distribution between the Base and the Support.

		Base $l_{b,x}$ [m]				
		1.00	1.10	1.20	1.30	1.40
Support $l_{s,x}$ [m]	0.11					x
	0.21				x	
	0.31			x		
	0.41		x			
	0.51	x				

As can be seen in figure 4.4 the total displacement does not deviate much if the length is being re-distributed vertically.

4.1.2 Parametric analysis of the masses

Here it is investigated what effect each individual mass has on the performance of the system. The range is percent-relative to value: A range of -20% and +20% for each mass is used. Each time, five default levels have been calculated.

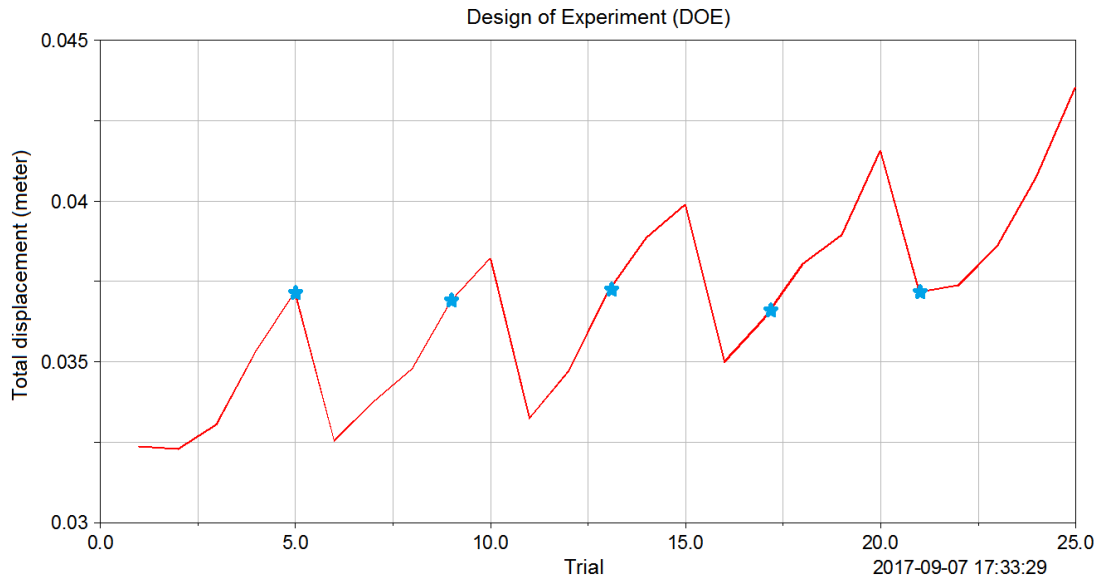
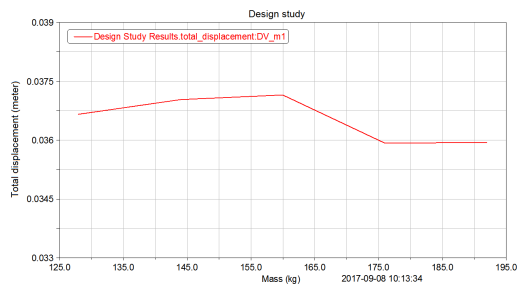


Figure 4.4: 25 possibilities of the vertical length re-distribution between the Base and the Support. The blue asterixes match with the "x's" in table 4.5. Combination trial on horizontal axis and performance measure on vertical axis.

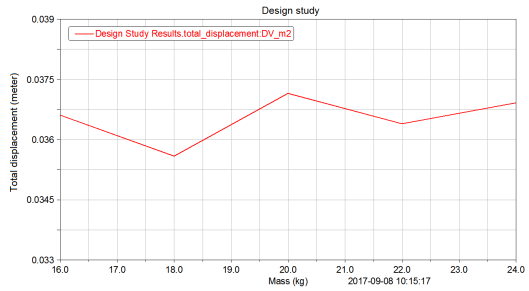
Table 4.6: Initial masses of the model of the microscope support system.

Mass	[kg]
Base	160.0
Support	20.0
Arm	35.0
Yoke	7.0
Microscope	10.0

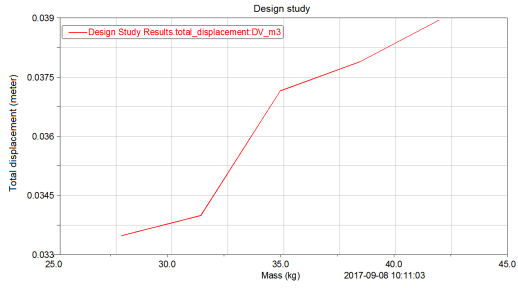
Clearly, the total displacement increases when the mass of the Arm is increased. The total displacement does not show any correlation with altering the mass of the Base, Support, Yoke and Microscope. However, the fundamental frequency of the system increases significantly ($m_{mic} = 10 \text{ kg} : f_n = 3.01 \text{ Hz}$ and $m_{mic} = 12 \text{ kg} : f_n = 2.89 \text{ Hz}$) which results in an increased settling time.



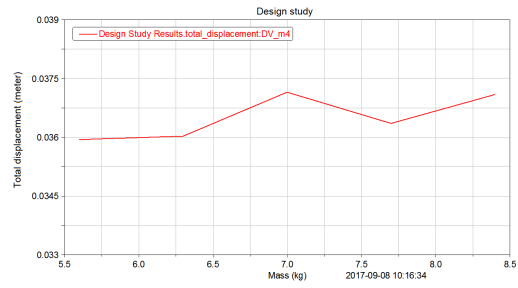
(a) Mass analysis of the Base.



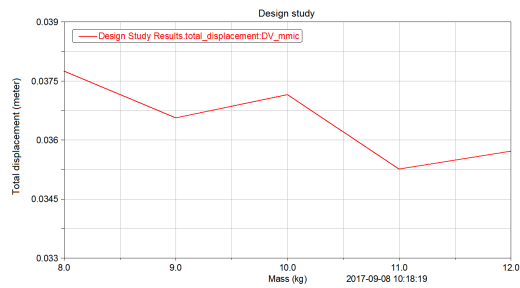
(b) Mass analysis of the Support.



(c) Mass analysis of the Arm.



(d) Mass analysis of the Yoke.



(e) Mass analysis of the Microscope.

Figure 4.5: Results of the parametric analysis of the masses. Masses on horizontal axis and performance measure on vertical axis.

Re-distribution of the Yoke and Arm masses: Again, for valid re-distribution an absolute-relative value is used instead of a percent-relative: A range of -2 to +2kg is used. Five default levels for both masses are calculated which results in the matrix in table 4.7. Only the diagonal terms contain an overall mass equal to the original mass.

Table 4.7: Valid mass re-distribution between the Yoke and the Arm.

		Mass of the Yoke				
		5	6	7	8	9
Mass of the Arm [kg]	33					x
	34				x	
	35			x		
	36		x			
	37	x				

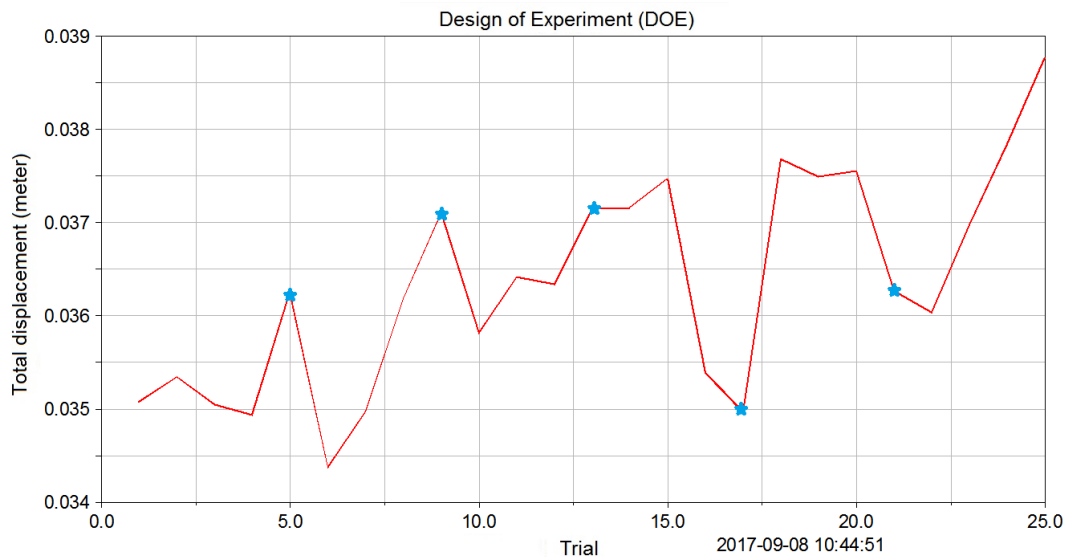


Figure 4.6: 25 possibilities of the mass re-distribution between the Arm and the Yoke. The blue asterixes match with the "x's" in table 4.7. Combination trial on horizontal axis and performance measure on vertical axis.

The total displacement of the microscope for these five diagonal terms are displayed with blue asterisks in the graph. According to this graph, the ideal mass distribution is the situation with masses of the Arm and Yoke respectively 36 kg and 6 kg.

4.1.3 Parametric analysis of the torsion stiffnesses

Investigate what effect each individual stiffness has on the response of the system. The initial values are displayed in table 4.8.

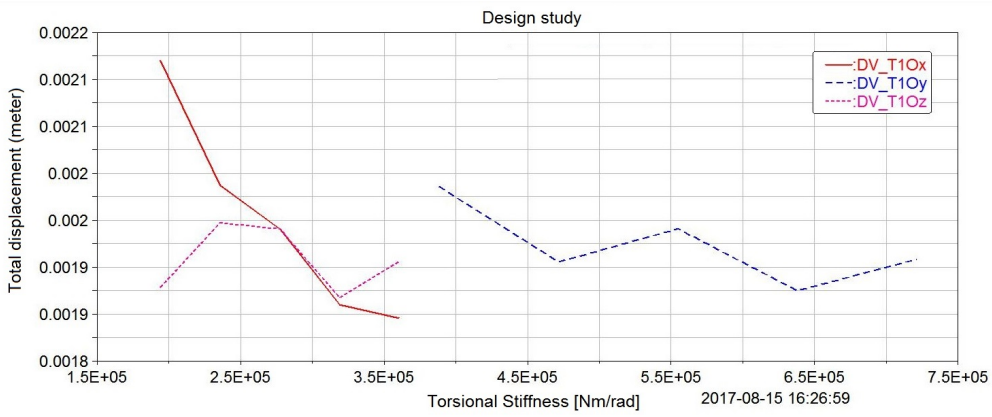
Table 4.8: Initial torsional stiffnesses in the four joints of the model of the microscope support system.

Stiffness	[Nm/rad]
TO _x (TO _z)	2.78E+05
TO _y	5.55E+05
TA _x	9.25E+05
TA _y	5.55E+04
TA _z	3.15E+05
TB _x	9.25E+03
TB _y	2.59E+04
TB _z	3.52E+04
TC _x	9.25E+03
TC _y	2.41E+04
TC _z	3.88E+04

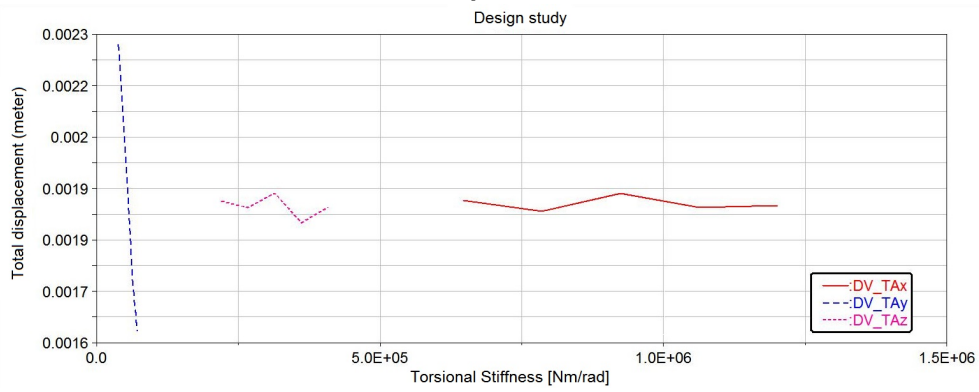
Figure 4.7 shows the influence of adjusting each torsions stiffness individually. The range is percent-relative to value: A range of -20% and +20% for each stiffness is used. Each time, five default levels have been calculated.

The graphs display the effect on the total displacement for the modifications on the three torsional stiffnesses in each joint. This way, the scaling on the y-axis does not give a misleading view on the effect. More or less horizontal lines imply a limited influence of that particular adjustment. Lines from top left to bottom right imply an improved system regarding the total displacement when that particular stiffness is increased. Lines from the bottom left to top right imply an improved system regarding the total displacement when that particular stiffness is decreased.

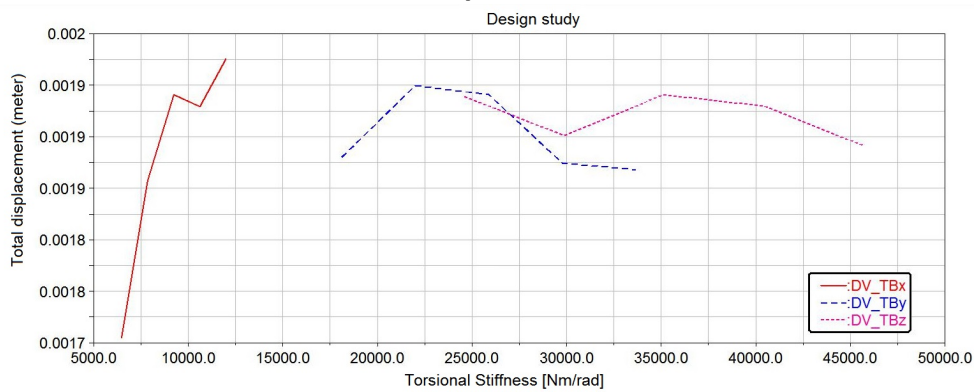
Design variables TO_x, TO_y and TA_y behave as expected: A higher stiffness results in a lower total displacement of the microscope. This effect is displayed in figure 4.8 with the microscope z-displacement for K_y of joint A equal to the initial value 9.25E+03 and half of this value: 4.625E+03. Adjustments to the design variables TB_x and TC_x show the opposite effect: A lower stiffness improves the system regarding the microscope displacement. To further investigate this effect, a graph is made of the microscope z-displacement with K_x of joint B equal to the initial value 9.25E+03 and half of this value: 4.625E+03 (figure 4.9). It can be seen that the response after removal of the force is indeed improved: The oscillations damp out quicker. However, the static displacement increases too which makes the system less robust.



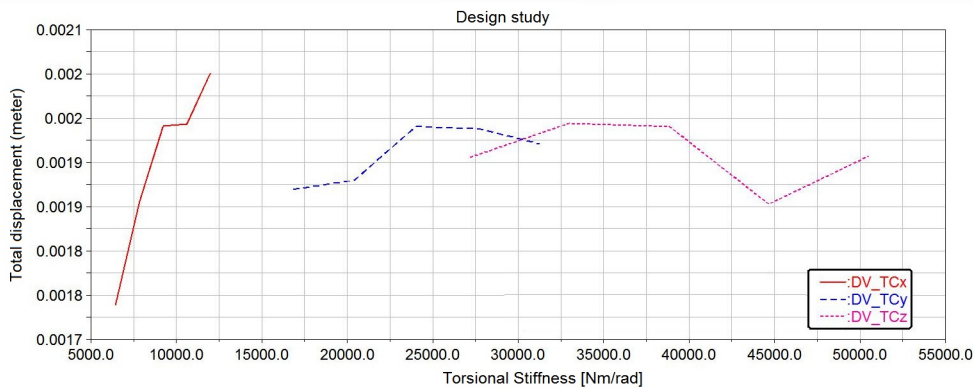
(a) Joint O: K_x (red), K_y (blue) and K_z (magenta).



(b) Joint A: K_x (red), K_y (blue) and K_z (magenta).



(c) Joint B: K_x (red), K_y (blue) and K_z (magenta).



(d) Joint C: K_x (red), K_y (blue) and K_z (magenta).

Figure 4.7: Results of the parametric analysis of the torsion stiffnesses. Stiffness on horizontal axis and performance measure on vertical axis.

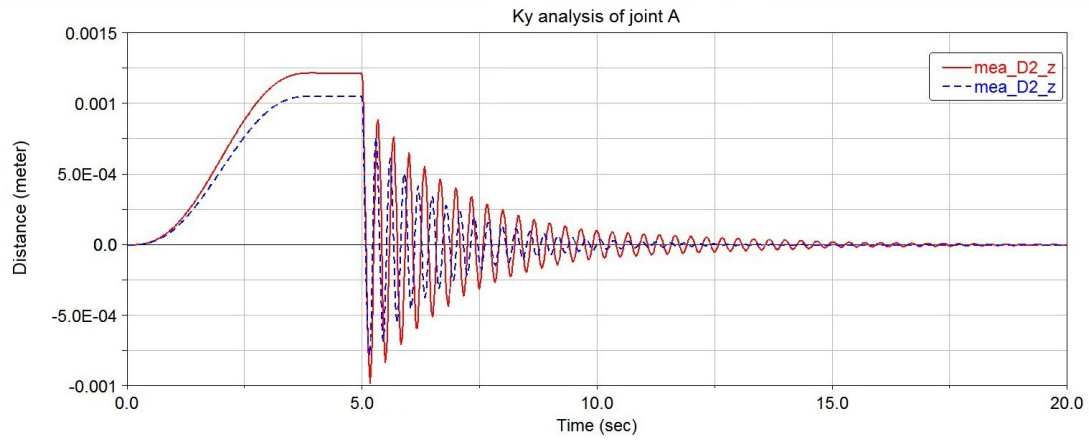


Figure 4.8: Measure on the displacement of the microscope for K_y of joint A equal to 5.55×10^4 (red) and 1.10×10^5 (blue dotted).

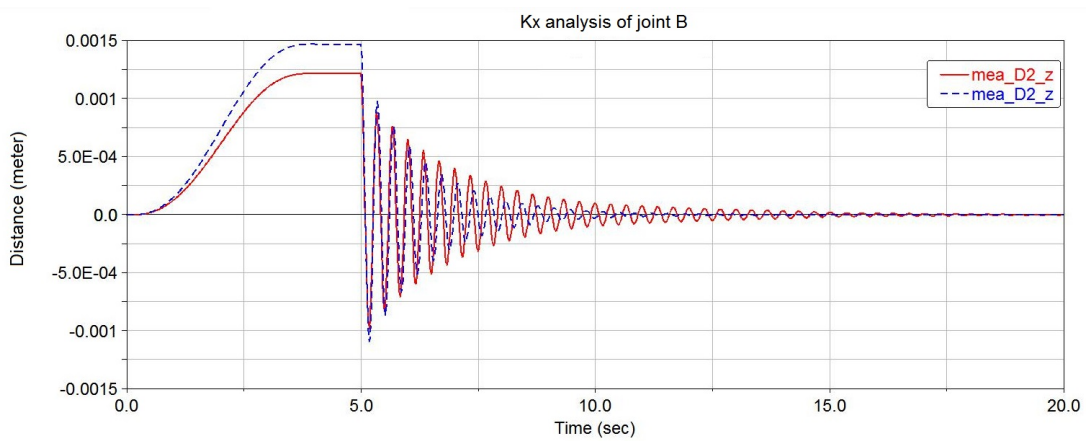


Figure 4.9: Measure on the displacement of the microscope for K_x of joint B equal to 9.25×10^3 (red) and 4.625×10^3 (blue dotted).

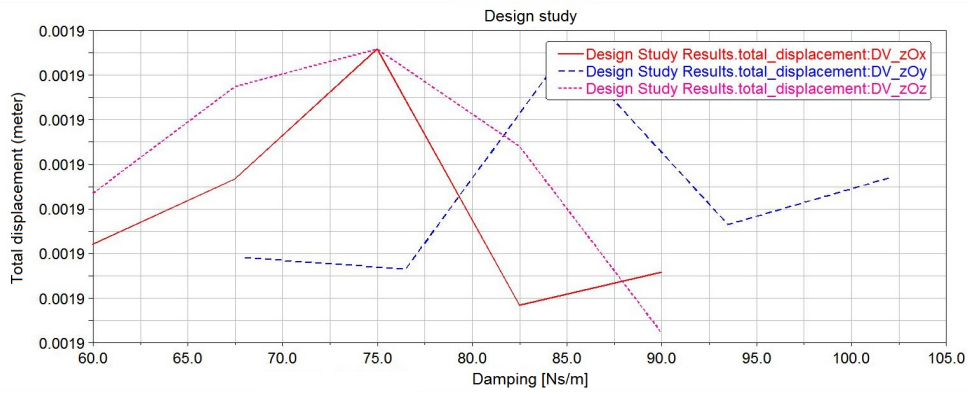
4.1.4 Parametric analysis of the torsion damping variables

Here it is investigated what effect each individual damping variable has on the response of the system. The initial values are displayed in table 4.9. Figure 4.10 shows the influence of adjusting each damping factor individually, grouped per joint. The range is percent-relative to value: A range of -20% and +20% for each factor is used. Each time, five default levels have been calculated.

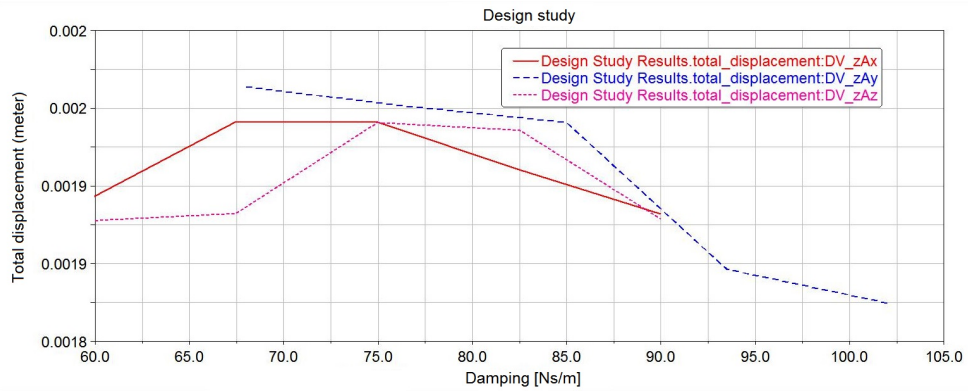
Table 4.9: Initial torsional damping constants of the model of the microscope support system.

Damping	[Ns/m]
z_{Ox} (z_{Oz})	75
z_{Oy}	85
z_{Ax}	75
z_{Ay}	85
z_{Az}	75
z_{Bx}	85
z_{By}	80
z_{Bz}	80
z_{Cx}	80
z_{Cy}	75
z_{Cz}	80

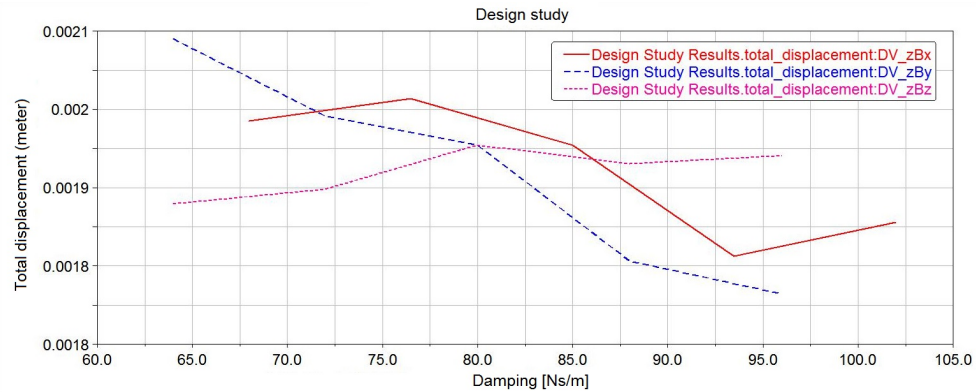
Design variables z_{Ay} , z_{By} and z_{Cx} show that with a higher damping coefficient a lower total displacement is achieved. The damping coefficients in joint O do not show much effect on the behaviour of the system (might be misleading due to the scaling of the vertical axis). The reason for this can be that the angular velocities in joint O are so small, that the virtual viscous damping coefficients don't have any effect.



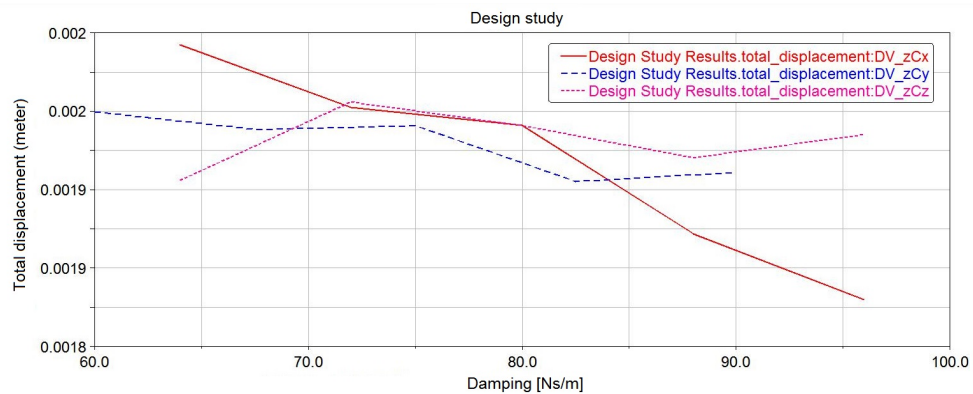
(a) Joint O: Z_x (red), Z_y (blue) and Z_z (magenta).



(b) Joint A: Z_x (red), Z_y (blue) and Z_z (magenta).



(c) Joint B: Z_x (red), Z_y (blue) and Z_z (magenta).



(d) Joint C: Z_x (red), Z_y (blue) and Z_z (magenta).

Figure 4.10: Results of the parametric analysis of the damping coefficients. Damping coefficient on horizontal axis and performance measure on vertical axis.

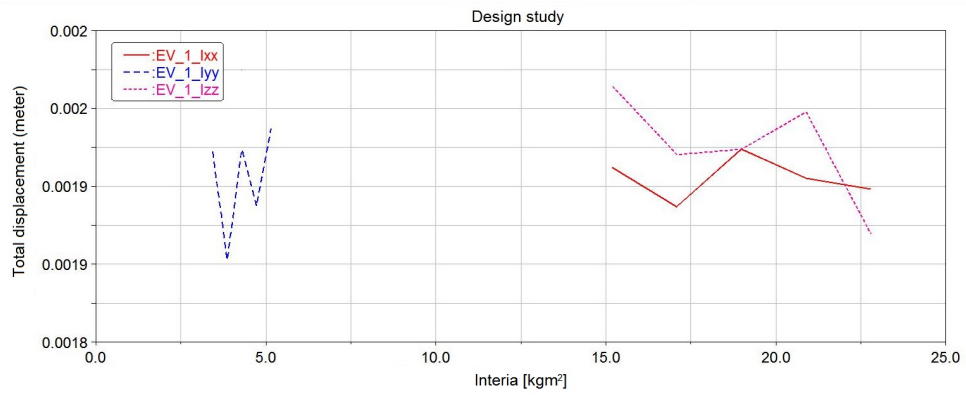
4.1.5 Parametric analysis of the link inertias

Here it is investigated what effect each individual inertia coefficient has on the response of the system. The initial values are displayed in table 4.10. Figure 4.11 shows the influence of adjusting each inertia individually, grouped by the link number. The inertia of the Microscope is displayed in the graph of Link 4. The range is percent-relative to value: A range of -20% and +20% for each inertia is used. Each time, five default levels have been calculated.

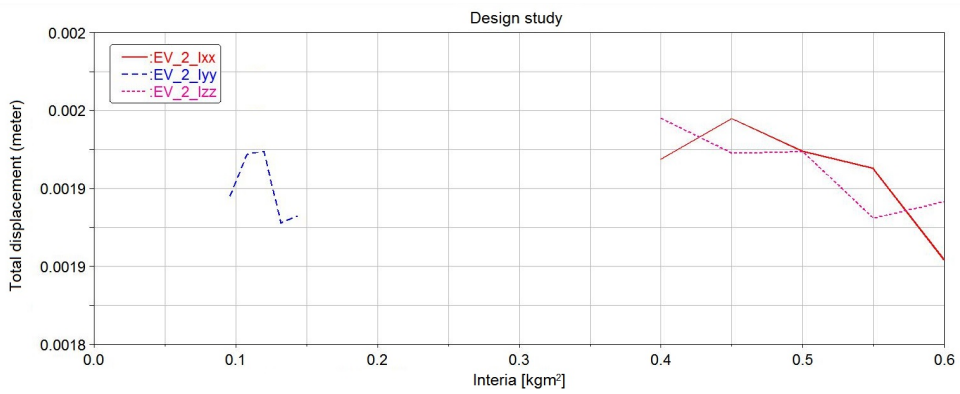
Table 4.10: Inertia coefficients of the model of the microscope support system.

Inertia	[kgm ²]
Link 1-Ixx (1-Izz)	19
1-Iyy	4.3
Link 2-Ixx (2-Izz)	0.5
2-Iyy	0.12
Link 3-Ixx	0.5
3-Iyy (3-Izz)	2.37
Link 4-Ixx (4-Izz)	0.2
4-Iyy	0.05
5-Imic	0.1

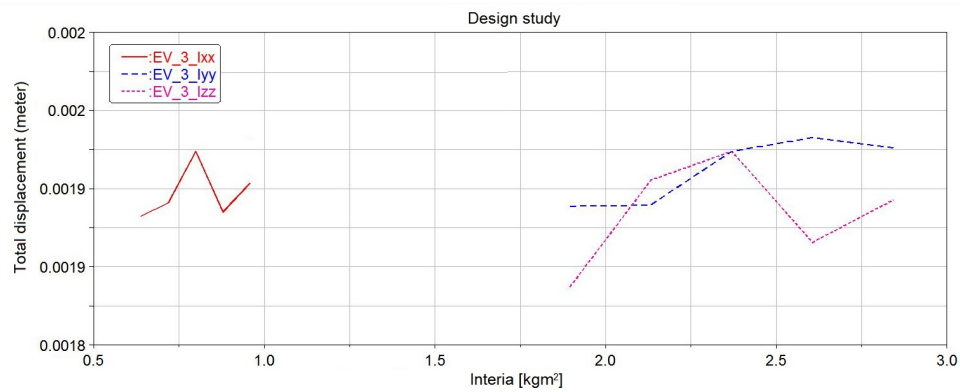
From the graphs it can be concluded that none of the inertias really affects the performance of the system. The variation of the results can be attributed to noise and is this large due to the scaling of the vertical axis. The five varied inertias of the microscope lie in a completely horizontal line, because it has been modelled as a sphere with its centre of mass located at joint D.



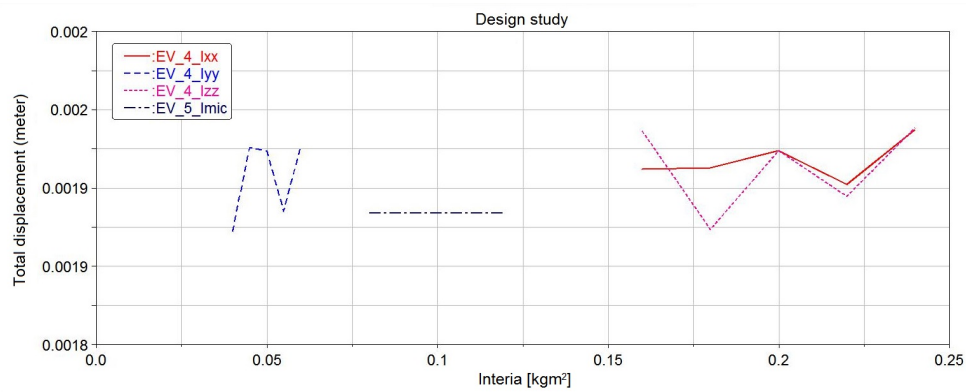
(a) Link 1: I_{xx} (red), I_{yy} (blue) and I_{zz} (magenta).



(b) Link 2: I_{xx} (red), I_{yy} (blue) and I_{zz} (magenta).



(c) Link 3: I_{xx} (red), I_{yy} (blue) and I_{zz} (magenta).



(d) Link 4: I_{xx} (red), I_{yy} (blue) and I_{zz} (magenta) and microscope I_{mic} (black).

Figure 4.11: Results of the parametric analysis of the link inertias. Inertia on horizontal axis and performance measure on vertical axis.

4.1.6 Parametric analysis of the relative position of the CoM

Here it is investigated what effect the position of the centre of mass of each link has on the response of the system. The position is calculated from a percentage of the link length. These percentages are displayed in table 4.11. Figure 4.12 shows the influence of adjusting each percentage individually. The range is absolute with limits of 10% and 90% for each factor. Each time, five default levels have been calculate

Table 4.11: Initial percentages of the positions of the CoM of the links.

Position	[%]
Base	0.2
Support	0.5
Arm	0.5
Yoke	0.5

It can be seen that adjusting the position of the Arm CoM results in the largest effect: Closer to the base lead to a lower total displacement of the microscope. The same counts for the CoM of the Base. Adjusting the position of the Yoke CoM shows an opposite effect: More mass closer to the microscope leads to a slightly lower total displacement. In figure 4.12 limits to the vertical axis have been set to visualize each design variable well.

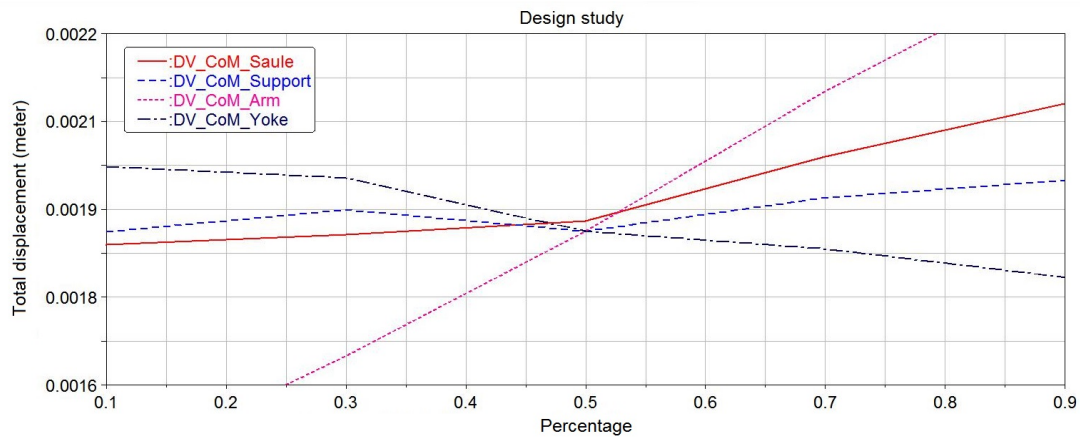


Figure 4.12: Altering each relative position of CoM between 10% and 90% of the link length. Percentage on horizontal axis and performance measure on vertical axis.

4.2 Multiple system configurations

One of the advantages of a simulated model is the ease of defining a new configuration and subsequently perform the same experiments. Not all experiments from section 4.1 will be repeated for different positions because this is too elaborate. Instead, a small selection of experiments will be repeated for different positions.

The properties of six different configurations, in the initial condition, are listed in table 4.12. The angles of axis 3 are chosen between plus and minus 20 degrees. In practice,

Table 4.12: Original model performance of different configurations.

Nr.	Configuration axis 1 and 2 [degrees]	Configuration axis 3 [degrees]	First natural frequency [Hz]	Damping ratio [%]
1	90	0	3.45	3.6
2	90	+20	3.63	2.6
3	90	-20	3.12	5.3
4	0	0	3.01	2.6
5	0	+20	3.13	2.1
6	0	-20	2.80	3.9

this is also more or less the range within axis 3 varies. More information on this angle can be found in section 4.3. Figure 4.13 shows the second and third configurations of the table for visualization.

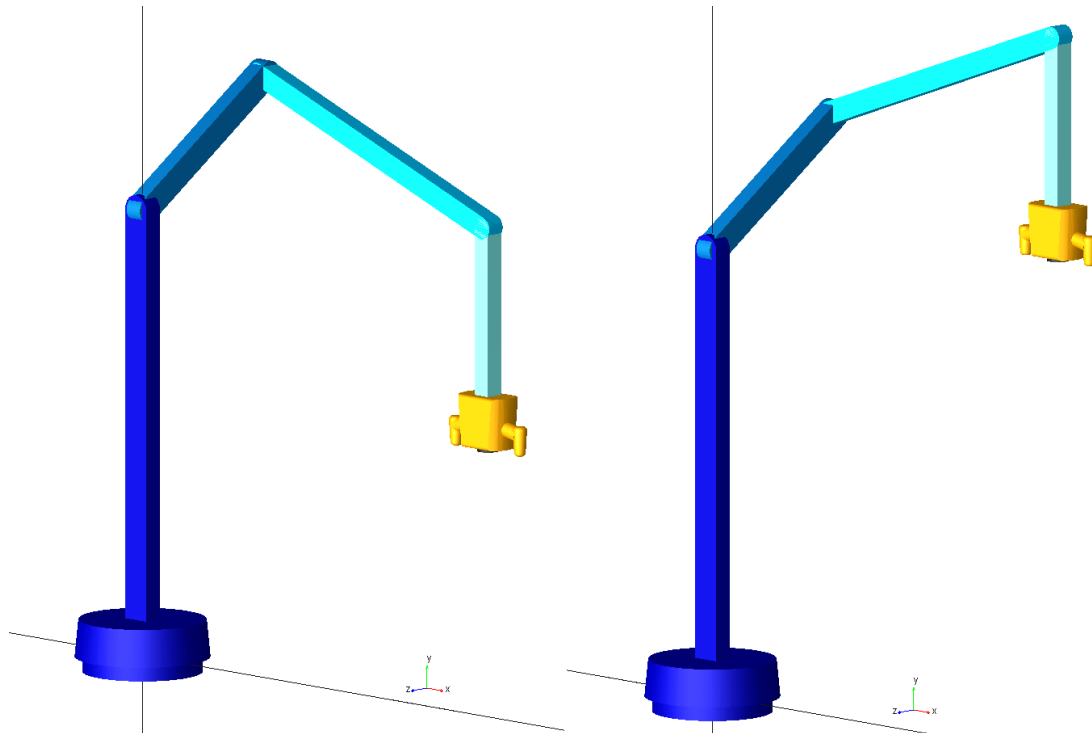


Figure 4.13: Model with axis 1 and 2 equal to 90° and axis 3 -20° (left) and 20° (right).

Varying the length of the Arm resulted in a major effect on the performance of the system. Therefore this variable is used to show the effect of each of the six different configurations. Again, a range of plus and minus 20% is used and five default levels are calculated each time.

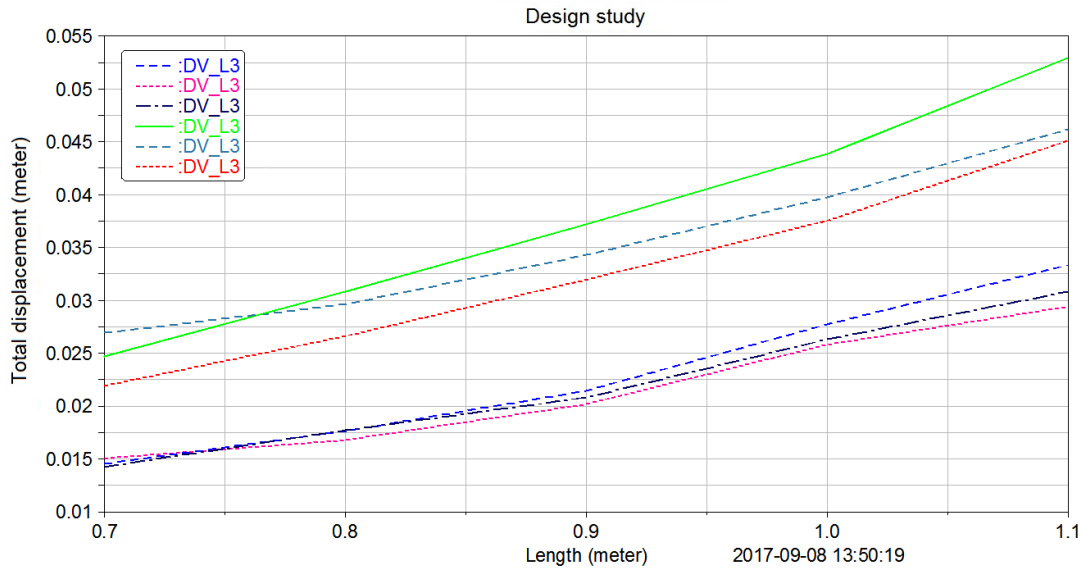
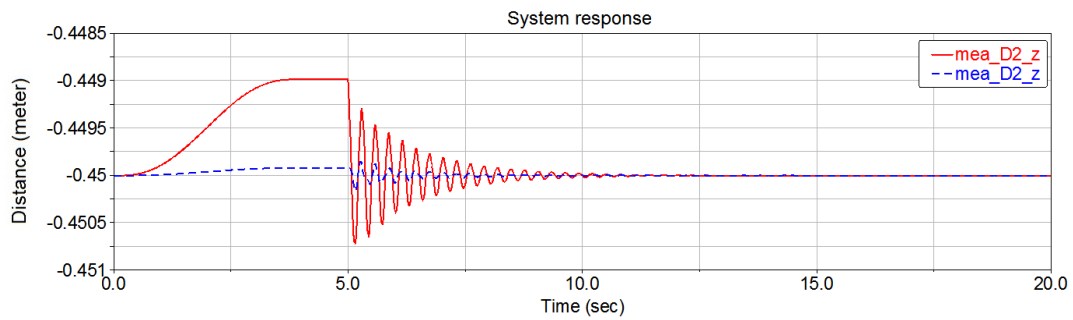


Figure 4.14: System performance of six configurations when length of Arm is altered. The sequence in the legend in the figure matches the sequence of configurations in table 4.12: Blue is configuration nr. 1, mangenta is configuration nr. 2, etc.

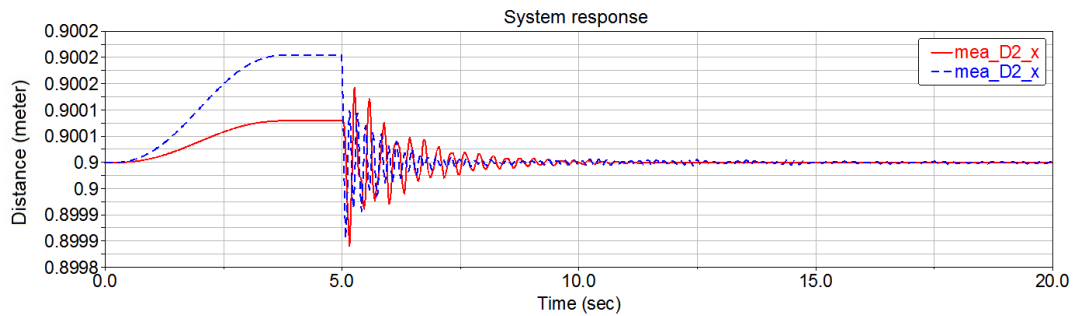
In figure 4.14 the results are displayed in the same order as in table 4.12. A similar behaviour is found for each configuration. In the "90 degree" configuration the effect on the performance is less when axis 3 is being adjusted compared to the "straight" configuration.

4.2.1 Other direction of applied force

This whole chapter, the force was applied in z-direction. This was done because the vibrations in this situation were, by far, the greatest. This is confirmed in the system response displayed in figure 4.15. It does not matter whether the vibrations are measured in z-direction (upper graph) or x-direction (lower graph), for both the vibrations are the greatest when the force is applied in z-direction (red), even though the static deflection in x-direction is greater for a force applied in this direction as well. These graphs are made with the model in configuration nr.1. The difference in vibration response is even better visible with model configuration nr. 4.



(a) Displacement-time graph of the system response, measured in z-direction at point D, force applied in z-direction (red) and in x-direction (blue dotted).



(b) Displacement-time graph of the system response, measured in x-direction at point D, force applied in z-direction (red) and in x-direction (blue dotted).

Figure 4.15: Effect of the direction of the applied force and the direction of the measurement. Model configuration 1.

4.3 Valid parameter range in practice

The experiments in this chapter have mostly been executed with relative parameter ranges of -20% and 20%. In practice these modifications are often violating the requirements when implemented. This section will give an overview of the parameter ranges that are allowed such that one valid maximally improved system can be simulated in section 4.4. This overview will be given in the same order as implied with table 4.2.

The lengths of the links can only be changed if the absolute position of the microscope does not change. This can be achieved when lengths are interchanged and this has already been investigated: From figure 4.3 and 4.4 it can be seen that only redistributing length horizontally improves the performance. However, enlarging the Support length relative to the Arm length, shortens the reach of the system in the "90 degree" configuration. Besides that, a shorter Arm will complicate the design when the same vertical reach is required. The lengths will therefore not be adjusted, but it should be kept in mind that the effect on the performance is great (see figure 4.1). If the surgeons accept a smaller reach of the total support system the dynamic performance will be higher.

The masses of the links and the microscope are also limited to changes. Figure 4.5c clearly shows that the Arm should have a mass as low as possible. Up to a certain level, this can be realized by material choice and design considerations, but my experience is that Hittech Multin already puts great effort in lowering the mass of their designs. The modularity of the microscope itself(extra oculars, extended oculars, camera, etc.) results in a microscope mass range of 9 kg to 12 kg.

Stiffness adjustment does not only affect the dynamic response but also the static response as showed in figure 4.9. Therefore, the stiffness in joint B and C should not be lowered to improve the dynamic performance if the static performance is not allowed to decrease. In other words: If the robustness of the support system persists to be a requirement, the stiffnesses in joint B and C cannot be lowered. A total different situation is found with joint O and A: Performance improvements can be made effectively if the bending stiffness in joint O and A are increased (See figure 4.7a and 4.7b). Increasing these stiffnesses does not negatively affect the static performance so it's a win-win situation. However, making them stiffer might result in a heavier and less slender system or require more expensive connections. The influence on the vibrational behaviour might also be greatly affected by the casters and the hospital floor. This is left for future investigations.

Adjustments to the damping coefficients are the most obvious ways to improve the dynamic performance of the system, but in practice, damping is not as easily added as in the model. Adding friction in a joint or adding a viscous piston between two links affects the requirement of fluent repositioning and therefore will this not be treated further.

The experiments with the inertias did not show much effect on the performance of the system. From a simple compound pendulum it is known that when the inertia is increased, the acceleration decreases and the period increases. A mass distribution along the link that increases its inertia would therefore result in a lower performance. Apparently the effect is small according to graphs in figure 4.11.

Adjusting the position of the centre of mass showed some effect on the performance of the system. In practice, the absolute range cannot be all the way between 10 and 90% as in figure 4.12, but a feasible range is 25%. Bodywork, knobs, internal electronics and other features in and on the support system can be moved along the length of the link.

Finally, the rotational ranges of each joint are discussed here. They do not count as parameters suited for dynamic experiments, but they are of importance for the initial positions of the system. These ranges are obtained from the brochure and CAD models and are listed in table 4.13.

Table 4.13: Ultimate angle positions of each joint.

Joint number	Range [degrees]
1	± 360
2	-170 to +145
3	-20 to +55
4	± 270
5	± 46
6	-75 to +125

4.4 Combined maximum improvement

A new set of system parameters is created from combining the separate improvements found with the experiments and respecting the valid ranges. The performance of this new system will be compared to the performance of the original system. It can be seen

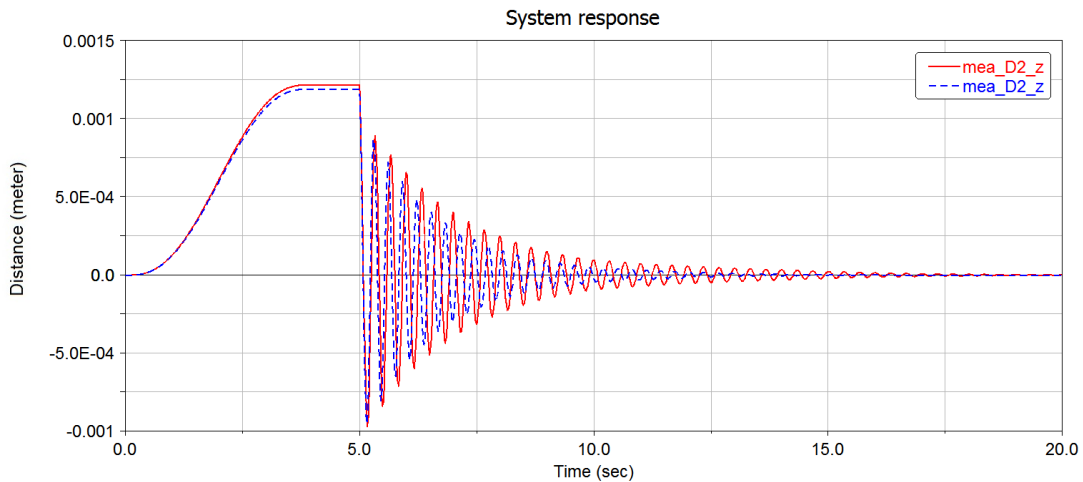


Figure 4.16: Measure on the displacement of the microscope of the original system (red) and the improved new system (blue dotted). This graph is made in configuration 4, as an example.

that the adaptations result in a system with lower-amplitude vibrations and that returns quicker to its equilibrium position. Moreover, the static performance is slightly

improved as can be seen in the graph between three and five seconds.

The average settling time of the original system amounts 6.42 seconds and is calculated with equation 1.4.1 and system properties obtained from column four and five of table 4.12. Running the simulation with the new parameters for all six configurations results in the values from table 4.14. With these new system properties and equation

Table 4.14: Improved model performance of different configurations.

Nr.	Configuration axis 1 and 2 [degrees]	Configuration axis 3 [degrees]	First natural frequency [Hz]	Damping ratio [%]
1	90	0	3.64	4.2
2	90	+20	3.86	3.0
3	90	-20	3.25	5.8
4	0	0	3.20	3.1
5	0	+20	3.37	2.3
6	0	-20	2.95	4.5

1.4.1 the 2%-settling time can be calculated and averaged which results in the value of 5.29 seconds.

The overall improvement of the system can be calculated with equation 4.4.1.

$$\left(\frac{5.29 - 6.42}{6.42} \right) 100\% = -17.5\% \quad (4.4.1)$$

All improvements combined and without violating the range defined in section 4.3 results in an improvement of 17.5% which means that the goal of 20% almost has been reached.

A side-note should be made concerning the combined improvement: Combining all the improvements of the separate analyses from section 4.1 does not automatically mean that this is the best solution. There might be other combinations of parameters that have a lower total displacement. However, by grouping the parameters, a better understanding of each effect is obtained compared to one optimization with brute force calculation.

5

Tuned mass damper

In the analysis process, the microscope support systems appeared to be principally equivalent to a simple cantilever beam clamped at one end and free at the other end. The largest deflection from the equilibrium position of a cantilever beam is always the point at the free end of the beam. Concerning the microscope support system, the microscope itself is located at the free end which will deflect the most. Equivalent systems of a cantilever beam can be imagined, such as rigid links connected by rotational joints with torsional springs or a translational system (figure 5.1b).

From this last representation the idea arose that a very straightforward way to lower the deflection of the microscope from its equilibrium position is to add another mass at the end that now deflects the most. The microscope itself subsequently deflects less than the system without the additional mass. This is a well known passive damping technique in civil engineering and is called a tuned mass damper (TMD). It is an elegant and simple solution for major amplitude reduction within a certain range of structural frequencies. Some current applications of TMD's are skyscrapers, bridges and high chimneys.

I visited Flow Engineering, a company in the Netherlands that designs and fabricates tuned mass dampers for civil structures[14]. They gave me general info on the working principle of TMD's and how they design them. We discussed the vibrational problem with the surgical microscope support system and their first impression was that it would be possible to design a suitable TMD. The calculation strategy used in this chapter is based on these instructions.

5.1 Tuned mass damper design

The parameters for the design of a tuned mass damper can be obtained with the Den Hartog method[15]. The total system should be represented as one translational spring-mass-damper system. The effective mass, the equivalent stiffness and the structural damping constant need to be calculated. The position of the TMD highly effects the whole system which is explained in section 5.1.3.

5.1.1 Equivalent single-degree-of-freedom system

First, the structure itself needs to be transformed to an equivalent single degree of freedom system. The distributed mass of the total system is reduced to a single point mass at a certain location. This location is the same as the location where the tuned mass damper is going to be placed and needs to be determined on beforehand (see section 5.1.3).

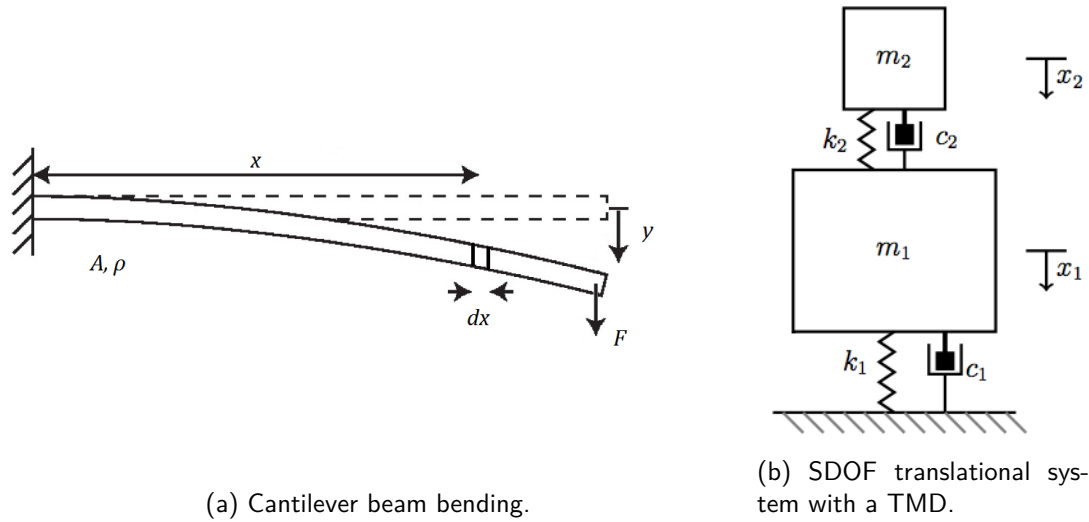


Figure 5.1: Surgical microscope support systems

Imagine a cantilever beam with cross section A , density ρ and stiffness in y -direction k_y subjected to a transverse force (figure 5.1a). With Rayleigh's method the effective mass of such a beam can be calculated. Rayleigh assumed that the potential energy stored in the flexure at maximum displacement is equal to the kinetic energy of the entire structure when it is moving at its maximum velocity [16]. The potential and kinetic energy are:

$$E_{p,max} = \int_0^l k_y dy = \frac{1}{2} k_y y_{max}(l)^2 \quad (5.1.1)$$

$$E_{k,max} = \int_0^l \frac{1}{2} \rho A v(x)^2 dx = \frac{1}{2} \rho A \omega^2 \int_0^l y(x)^2 dx \quad (5.1.2)$$

Stating that these equations are equal and rearranging for the resonant frequency gives:

$$\omega^2 = \frac{\frac{1}{2} k_y y_{max}(l)^2}{\frac{1}{2} \rho A \int_0^l y(x)^2 dx} = \frac{k_y}{m_{eff}} \quad (5.1.3)$$

The effective mass is defined as:

$$m_{eff,L} = \rho A \int_0^l \left[\frac{y(x)}{y_{max}(l)} \right]^2 dx \quad (5.1.4)$$

When the beam is assumed to be divided in a finite number of parts $—_j$, this relation can be rewritten in the form of equation 5.1.5. The position along the beam where the effective mass is desired is denoted by L , e.g. this does not have to be at the end of the beam.

$$m_{eff} = m_j \left(\frac{y_j}{y_L} \right)^2 \quad (5.1.5)$$

In case of the microscope support system, the effective mass at the desired location can be calculated as well. The desired location can best be chosen as close to the free end as possible (further explained in section 5.1.3).

The masses of each link of the model are listed in table 4.1. The deflections of each link's centre of mass of the model are listed in column two of table 3.2. In equation 5.1.6 the equivalent mass is calculated with the location of the TMD chosen at the centre of mass of the Yoke (So y_L is equal to the deflection at the CoM of link 4).

$$m_{eff} = 160 \left(\frac{9.2E - 03}{0.94} \right)^2 + 20 \left(\frac{0.12}{0.94} \right)^2 + 35 \left(\frac{0.45}{0.94} \right)^2 + 7 \left(\frac{0.94}{0.94} \right)^2 + 10 \left(\frac{1.22}{0.94} \right)^2 = 32.2\text{kg} \quad (5.1.6)$$

The equivalent stiffness is calculated in equation 5.1.7.

$$k_{eq} = \frac{F_z}{\delta_{CoM,Yoke}} = 10639\text{N/m} \quad (5.1.7)$$

From these two parameters, the natural frequency of this SDOF system can be obtained:

$$\omega_1 = \sqrt{\frac{k_{eq}}{m_{eff}}} = 2.89\text{Hz} \quad (5.1.8)$$

The structural damping of the microscope support system model in configuration nr. 4 is 2.6%. As an overview, table 5.1 shows all parameters of the equivalent single-degree-of-freedom system.

Table 5.1: SDOF system parameters

m_1	32.2 kg
k_1	10 639 N/m
ω_1	2.89 Hz
ζ_1	0.026

5.1.2 Den Hartog method: optimal TMD design

Den Hartog derived the equations (5.1.9 and 5.1.10) for TMD design in 1956. The first equation calculates the optimal frequency ratio $q = \frac{f_2}{f_1}$ and the second calculates the

optimal damper coefficient. Structural damping was not included in these equations. Abubakar et al.[17] derived equations that generalize the computation of optimum design parameters for the TMD by including the effect of structure damping. Numerically optimization and curve fitting were used to obtain the equations 5.1.11 and 5.1.12. These last two equations will be used in this thesis, because a structure damping of 2.6% is quite high and cannot be neglected. As a reference, a steel beam clamped at one end can easily have a structural damping that is ten times lower[14].

$$q_{opt} = \left(\frac{1}{1 + \mu} \right) \quad (5.1.9)$$

$$\zeta_{2opt} = \sqrt{\frac{3\mu}{8(1 + \mu)}} \quad (5.1.10)$$

The parameter μ is a certain chosen mass ratio and gives the mass m_2 of the TMD: $\mu = \frac{m_2}{m_1}$. Usually this parameter is chosen between the 1 and 10% with a higher effect for higher values of μ . More explanation about the effects of choice of μ can be found in section 5.1.4.

$$q_{opt} = \left(\frac{1}{1 + \mu} \right) \left(1 - 1.5906\zeta_1 \sqrt{\frac{\mu}{1 + \mu}} \right) \quad (5.1.11)$$

$$\zeta_{2opt} = \sqrt{\frac{3\mu}{8(1 + \mu)}} + \frac{0.1616\zeta_1}{1 + \mu} \quad (5.1.12)$$

All parameters of the TMD can now be calculated. In table 5.2 this has been done for three values of μ to get a feeling what influence this has on the TMD parameters.

Table 5.2: "Optimal" TMD parameters in configuration 4, for μ equal to 10%, 5% and 1%

	for $\mu = 0.10$	for $\mu = 0.05$	for $\mu = 0.01$
q_{opt} [-]	0.898	0.944	0.986
m_2 [kg]	3.22	1.61	0.322
k_2 [N/m]	853	474	103
ω_2 [Hz]	2.59	2.73	2.85
ζ_{2opt} [-]	0.188	0.138	0.065

5.1.3 TMD placement

The location of the tuned mass damper can best be chosen as close to the free end as possible, to dissipate energy most efficiently. This is simply because the largest beam deflections occur here and the velocities are the highest here as well.

In case of the surgical microscope support system this is practically not possible. The microscope at the free end is not allowed to be modified and moreover, the microscope is able to rotate about axis 5 and axis 6 which results in a rotating TMD as well. Because the largest vibrations were measured in the horizontal plane, one wants to keep the TMD in this direction too.

The tuned mass damper becomes much less effective when it is placed further away

from the free end. From equation 5.1.5 it can be seen that this action results in a quadratically larger effective mass. Moreover, the deflection of a cantilever beam is expressed as in equation 5.1.13 and results in an even larger mass when the location is chosen further away from the free end.

$$y(x) = \frac{Fx^2}{6EI}(3L - x) \quad (5.1.13)$$

In reality, a suitable location for the tuned mass damper would be on the Yoke, because this link maintains a perpendicular orientation to the ground. There is also more space available for placement of the TMD. To prevent the support system from being asymmetrical and possibly unstable, the mass of the TMD should be spread evenly at the Yoke. This becomes more important for higher μ value selection. For example, a circle shaped ring around the Yoke can fulfil the role of the mass and flexures the role of the spring. These ring-shaped TMD's are also used on large chimneys.

5.1.4 Den Hartog method in practice

Den Hartog purely aims to find the optimum parameters of the TMD for one particular system. However, if the parameters of the main structure (microscope support system) change, the performance of the TMD can drop. In practice, the 'worst case' of the structure is being calculated and parameters for the TMD are chosen from a line diagram (see appendix A) such that the TMD damps this situation as desired. The "worst case" implies the situation where q is the lowest, so where the support system has the highest frequency compared to the frequency of the TMD. In this chapter a distinction is made between the "optimal" TMD calculation and "practical" TMD calculation.

Every other situation with higher q are damped as least as good as this worst case, as long as a certain range is respected. This range is dependent on the chosen mass ratio μ , the frequency ratio q , the structural damping ζ_1 and the physical possible/available damping ratio ζ_2 . It can be concluded that the Den Hartog method is the basis for TMD design, but in practice more considerations are required. How the line diagram from appendix A should be used will be explained in the next section along the example of the microscope support system.

5.2 Simulated microscope support system model and the tuned mass damper

In Appendix A the line diagram (Bierum circles) for $\mu = 0.10$ and $\zeta_1 = 0$ is displayed. It has been constructed by multiple Den Hartog calculations for many different initial conditions. The company Flow Engineering[14] created this diagram and diagrams with other initial conditions themselves and they are not publicly available. Although the structural damping $\zeta_1 = 0$ does not match with the 2.6% from the simulated model, explaining the design technique can be done just fine.

First, the situation with the highest support system frequency must be found. From table 4.12 it was found that the "90 degree", "+20" configuration has the highest first natural frequency (3.63 Hz). From the parametric analyses in chapter 4 it was found that this is the case for the microscope stripped from all its modules. Without the

second pair of oculars the microscope is 1 kg lighter and the first natural frequency in the mentioned configuration is then 3.69 Hz. The situation with the lowest support system frequency must also be calculated. From table 4.12 the value 2.80 Hz is obtained and with the maximum amount of modules added to the microscope (2 kg heavier) the lowest first natural frequency, according to the Adams model, is 2.67 Hz. The two q values can be calculated when a suitable eigenfrequency of the TMD, f_2 , is chosen. This acquires some trial and error and shifting of points in the line diagram to end up with the value of $f_2 = 2.80$ Hz, because for this value the range is nicely centred around the optimum value of $q = 0.91$ (see figure 5.2).

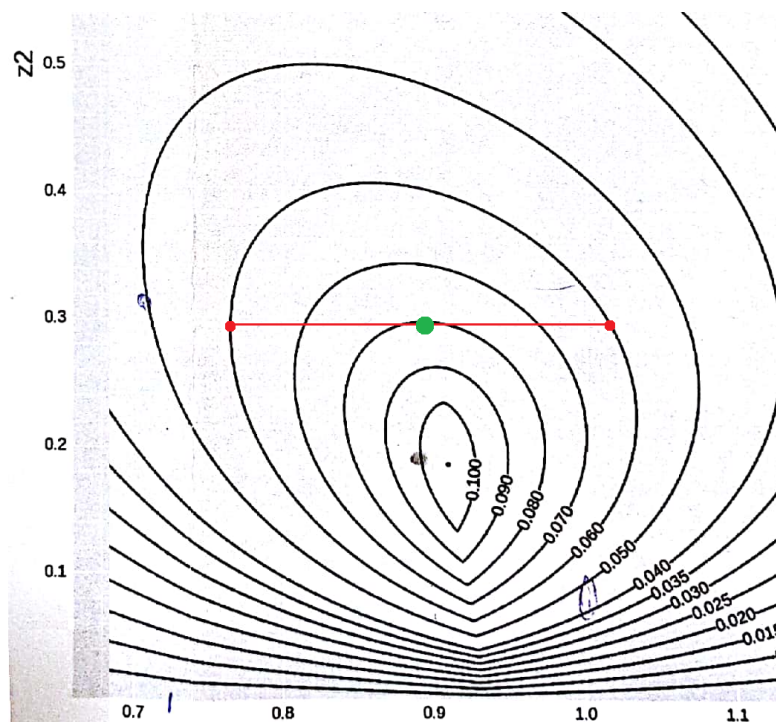


Figure 5.2: Enlarged picture of the line diagram of appendix A (created by Flow Engineering[14]). Mass ratio μ is equal to 10%. Frequency ratio q on the horizontal axis and the damping coefficient on the vertical axis. Added damping is written on each line. Left red dot: Frequency ratio for the highest support system frequency. Right red dot: Frequency ratio for the lowest support system frequency. The red line indicates the frequency range of the support system which experience an added damping of at least 6%.

From the line diagram it can be seen that an added damping of at least 6% over the whole range can be guaranteed, if a damper for the TMD can be found with a ζ of 29%. The red points in figure 5.2 are put at the corresponding worst case scenarios and the red line shows the range where 6% damping is guaranteed. An added damping of 6% is a huge improvement compared to the 2.6% structural damping. Moreover, in a certain configuration (green point), at $q = 0.89$ so $f_1 = 2.80/0.89 = 3.15$ Hz, the added damping is even 8%. These improvements are however theoretical, so they will be slightly lower in practice.

An overview can now be made from the TMD parameters for this situation. The mass and eigenfrequency are already mentioned, the stiffness can be calculated from these

two and the required damper of 29% is assumed to be real. The overview is given in table 5.3.

Table 5.3: Practical parameters for the TMD (configuration 4 and $\mu = 0.10$).

m_2	3.22 kg
k_2	997 N/m
ω_2	2.80 Hz
ζ_2	0.29

5.2.1 Model of the tuned mass damper

Adams is used to model an optimal TMD for configuration 4. The software is also used to model a practical TMD with the parameters found in the previous section in order to have a suitable TMD for every position. The TMD is modelled as a sphere fixed to a translational spring-damper module at the position of the CoM of the Yoke (see figure 5.3, TMD is displayed in gray).

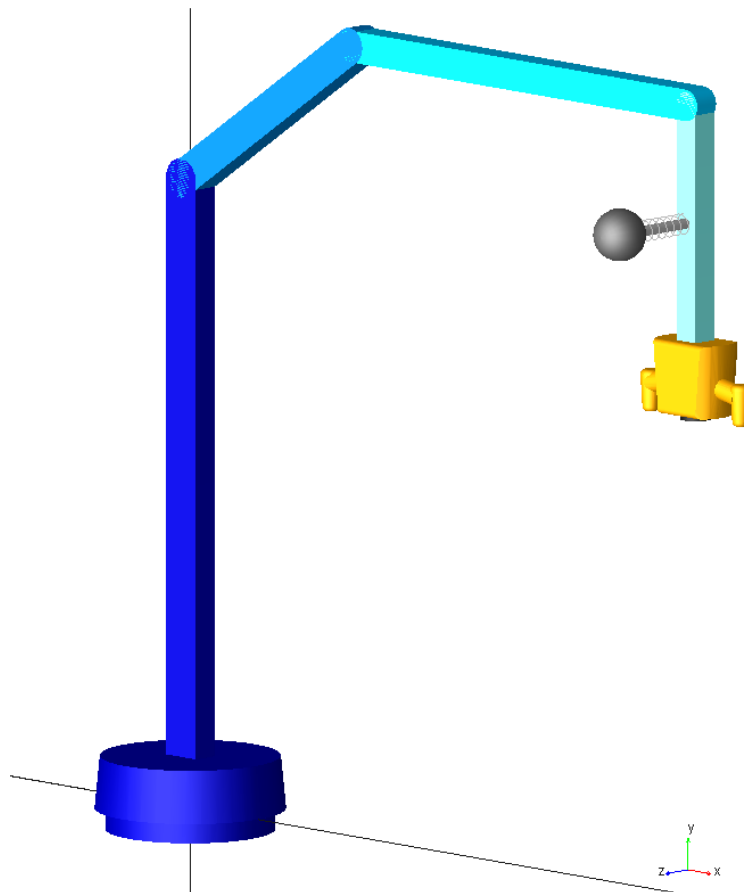


Figure 5.3: Tuned mass damper implemented in the Adams model. Spring-damper unit between the mass and the CoM of the Yoke.

Running the simulation and watching the support system and TMD move relative to each other already indicates that major improvements have been made. The result from the implementation of an "optimal" TMD (with parameters from the first column of table 5.2) in the model is displayed in figure 5.4. It shows the deflection of the microscope from the equilibrium position versus the time.

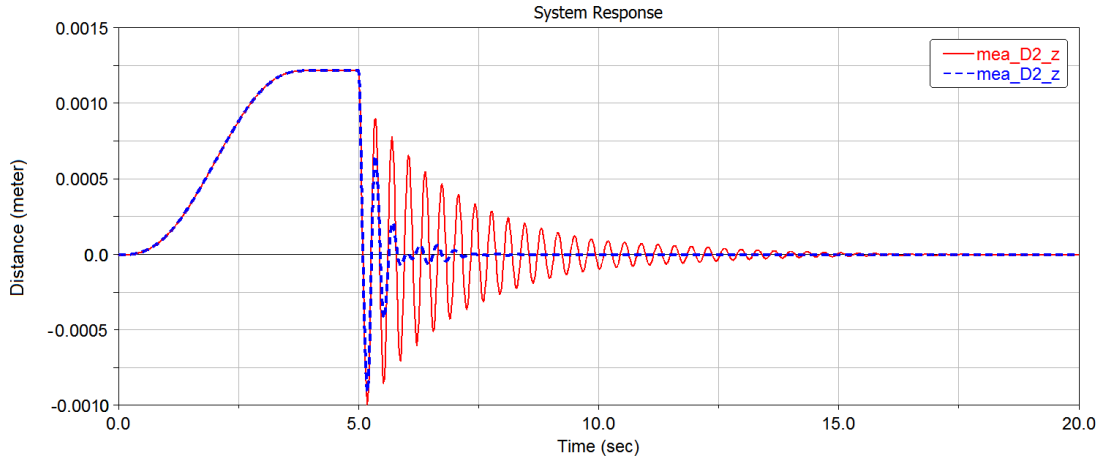


Figure 5.4: Response of the model (configuration 4) without TMD in red and with the "optimal" TMD in dotted blue.

Now, the parameters of the TMD will be adjusted following the variables in table 5.3: The "practical" TMD. This will result in a somewhat smaller improvement compared to the "optimal" TMD in configuration 4, but for other configurations, the practical system should be better than the optimal. The response of configuration 4 and 1 will be compared with graphs between these "practical" results and the "optimal" results. Indeed, the performance is slightly less when the blue and green line are compared in figure 5.5a, but the performance in the other configuration is better when the blue and green line in figure 5.5b are compared.

A quantitative comparison between the original system from table 4.12 and the system with the "practical" TMD will now be made. The system properties of the six configurations are listed in table 5.4.

Table 5.4: Properties of the model with a "practical" TMD.

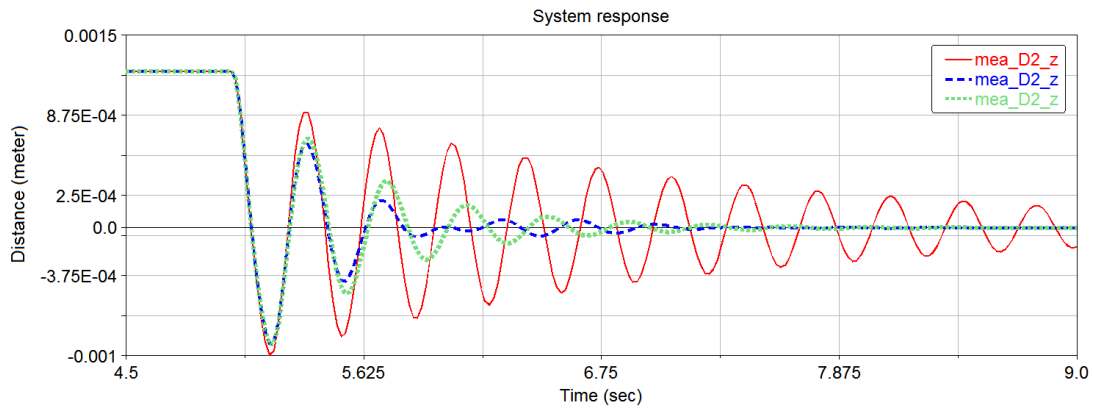
Nr.	Configuration axis 1 and 2 [degrees]	Configuration axis 3 [degrees]	First natural frequency [Hz]	Damping ratio [%]
1	90	0	2.74	22.6
2	90	+20	2.75	24.0
3	90	-20	2.69	17.1
4	0	0	2.70	13.5
5	0	+20	2.77	17.8
6	0	-20	2.51	10.3

The settling time of this new system can be calculated with equation 1.4.1 for each configuration and then averaged which results in the value of 1.45 seconds. The overall

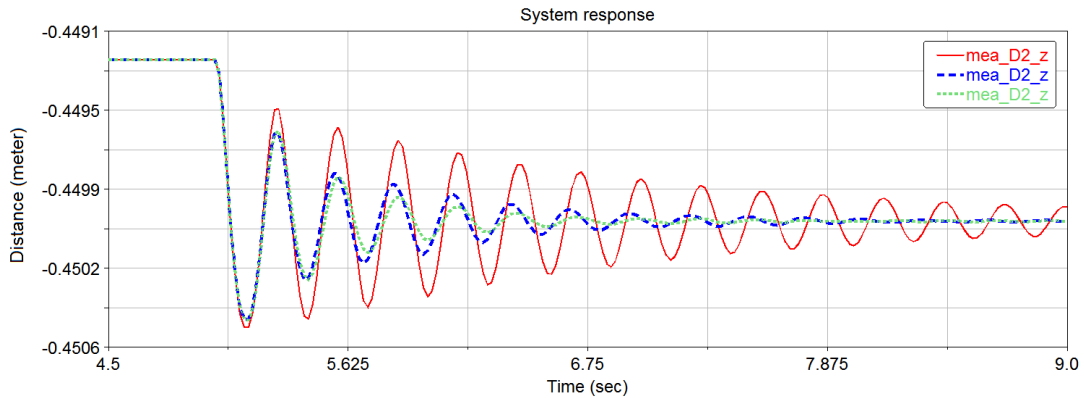
improvement of the system with a tuned mass damper can be calculated with equation 5.2.1.

$$\left(\frac{1.45 - 6.42}{6.42} \right) 100\% = -77.4\% \quad (5.2.1)$$

This settling time reduction greatly exceeds the target value of 20%, so an implementation of a TMD is highly recommended. The settling time reduction can also be calculated for lower TMD-masses when this is desired (column 2 and 3 of table 5.2). For indication, the average settling time with an optimal TMD with $\mu = 0.05$ is 2.26 seconds. The average settling time with an optimal TMD with $\mu = 0.01$ is 3.87 seconds. This results in overall settling time improvements of respectively 65.8% and 39.7%.



(a) Configuration Nr. 4: without TMD (red), with "optimal" TMD (blue) and with "practical" TMD (green).



(b) Configuration Nr. 1: without TMD (red), with "optimal" TMD (blue) and with "practical" TMD (green).

Figure 5.5: Response of two configurations to compare the two TMD design strategies.

6

Discussion and conclusion

The aim of this study was to reduce the settling time of the microscope support system when it is subjected to a step force caused by the surgeon after a repositioning action. The problem has been approached in two different ways: By a parametric analysis of modelled system parameters and by a simulated design of a subsystem with damping properties. These two methods will be compared in this chapter, followed by limitations and future work on this subject.

6.1 Comparison of two different improvement methods

The results of the parametric analysis from chapter 4 show that an improvement of 17,5% can be reached with adaptations to a small number of variables. Rather easy improvements to such a virtual model were not surprising: Bringing these improvements into practice is the challenge.

Obviously, settling time of a vibrating structure can be decreased when the damping coefficient and/or the natural frequency increases. From the basic formula $\omega = \sqrt{\frac{k}{m}}$ it can be suggested that, for example, increasing the stiffness of a cantilever beam will increase the natural frequency which results in higher velocities and therefore a lower settling time. One could say that there is no need for a virtual model when these basic formulas are in the back of the head of the engineer. However, the model showed great insight on what and how much effect each adaptation has.

The unexpected result was that the optimization objective S did not increase when the mass of the Yoke or the Microscope were increased. An explanation of this behaviour could be that the shape of the support system (Base and Support vertically upwards and Yoke downwards) affects the dynamic behaviour in a different way than expected. Adjustments to the Arm behaved as expected: Higher stiffness, lower mass and centre of mass closer to the fixed end result in a better performance. Adjustments to the Arm have the largest influence and are relatively easy to implement due to a larger design freedom, compared to the Yoke.

The results of support system with the tuned mass damper show a way more promising result. A TMD has been found that adds at least 6% damping to each tested configuration and with each microscope modules choice. For the six tested configurations and for the mass range of the microscope, the settling time improved with 77.4% on average. With a TMD, mass is counter-intuitively added to the free end of the support system to improve the overall behaviour of it. Usually, effort is put in lowering the mass in the design phase of such arms.

Tuning the TMD parameters such that the largest added damping takes place in the configuration that is used the most is also one of the possibilities. Even a TMD with an active system that adjusts its parameters can be realized. However, in my opinion, the beauty of the TMD lies in the fact that it is such a simple and passive system. The disadvantages of a TMD besides the added mass are the difficulty of suspending this mass and the rapid decreasing functionality if the damper property shifts. This is especially the case with viscous dampers that degrade by leaking. In further research, the type of dampers that are allowed in operation rooms must be selected and the required maintenance must be planned.

From the parametric analysis methods (section 2.1.4), only the first two have been used. The option in the Adams software to perform a real optimization has not been used, because there was not really a curve with a global minimum objective when a parameter was being adjusted. In hindsight, it was not a suitable project for such an analysis.

6.2 Modelling consequences: Errors due to simplifications

A model is a simplification of the reality. These simplifications result in differences between the model response and the response of the actual system. One of the main simplifications applied in this project was the assumption that the bending structure could be modelled with a limited number of rigid links interconnected with rotational joints. This type of modelling is valid when deflections are small. Rigid body modelling with large deflections is also valid, but then certain rules concerning PRBM must be respected[18].

Backlash (or play) due to clearances between parts has not been modelled. In hindsight it seemed to be of great influence on the actual system when studying the measurement results. If there had been another opportunity to perform experiments on the SCARA support system, the backlash could be understood and implemented in the model. Then, static equalization in section 3.1.1 would presumably show more similarities.

Friction in the joints has also not been modelled, but friction can be represented by equivalent viscous damping as explained in my literature study[1]. This representation is not fully concealed, because for very low velocities the damping is also low and the system keeps oscillating with small amplitudes. In reality, the static friction coefficient is larger than the kinetic friction coefficient, so at a certain point in time at a small level of oscillations, the relative motion between two links stays zero.

The resemblances between the model and an actual system in the section of the dynamic

validation imply that simplifications did not lead to significant errors. To support this hypotheses, it would be good to implement the improvements found in chapter 4 and 5 and measure the response of the actual support system.

6.3 Future work

The main recommendation would be the continuation with the design of a tuned mass damper. When a TMD with a value of $\mu = 0.10$ is acceptable, the exact shape of the mass and the type of springs and dampers should be chosen. In other cases with other values of μ , the calculations should be repeated as well.

If the goal of a follow-up study is to understand the behaviour of the support system better by building a more accurate model, the experimental strategy to obtain data from an actual microscope support system should definitely be improved. In future work, it would be good to set up an experiment with a functioning microscope in order to record vibrations visible through it. A stable microscope image is the purpose of this research. In this research, there was an extra boundary between vibrations at the microscope and the vibrations really visible through it. 'Boundary' implies the possible difference between the laser that measures the oscillations in one direction of the outer side of the microscope and the visible vibrations through the oculars. Oscillations recorded by the laser might not be noticeable on the microscope image and vice versa.

6.4 Conclusion

Two research paths were travelled to achieve the main objective of this master thesis: *Reduce the settling time of a surgical microscope support system with 20%*. It was found that with small adaptations to a limited amount of design variables, the goal nearly is reached. The allowed range in which the design can be varied is the limiting factor.

An improvement of over 75% was obtained when a tuned mass damper subsystem with a mass ratio μ of 10% was added to the support system model. Even with tuned mass dampers with a mass ratio of 5% or 1%, the goal was reached with ease.

With these findings the research question can be answered. *In which ways must the design of the support system be adapted to reduce its settling time without downgrading the functionality (e.g. robustness and ease of repositioning) of the support system?* The support system should be provided with a specifically designed tuned mass damper to reduce its settling time. The total operation time will be reduced significantly, when each repositioning action isn't paired with an extra delay of waiting for vibrations to die out.

7

Appendices

Appendix A: Line diagram for damping calculation when a TMD is added.

Appendix B: Labview block diagram.

Appendix C: Systems in Germany subjected to experiments.

Appendix D: Datasheet of the laser displacement sensor.

Appendix E: m-file used for processing the measurement data.

Appendix A

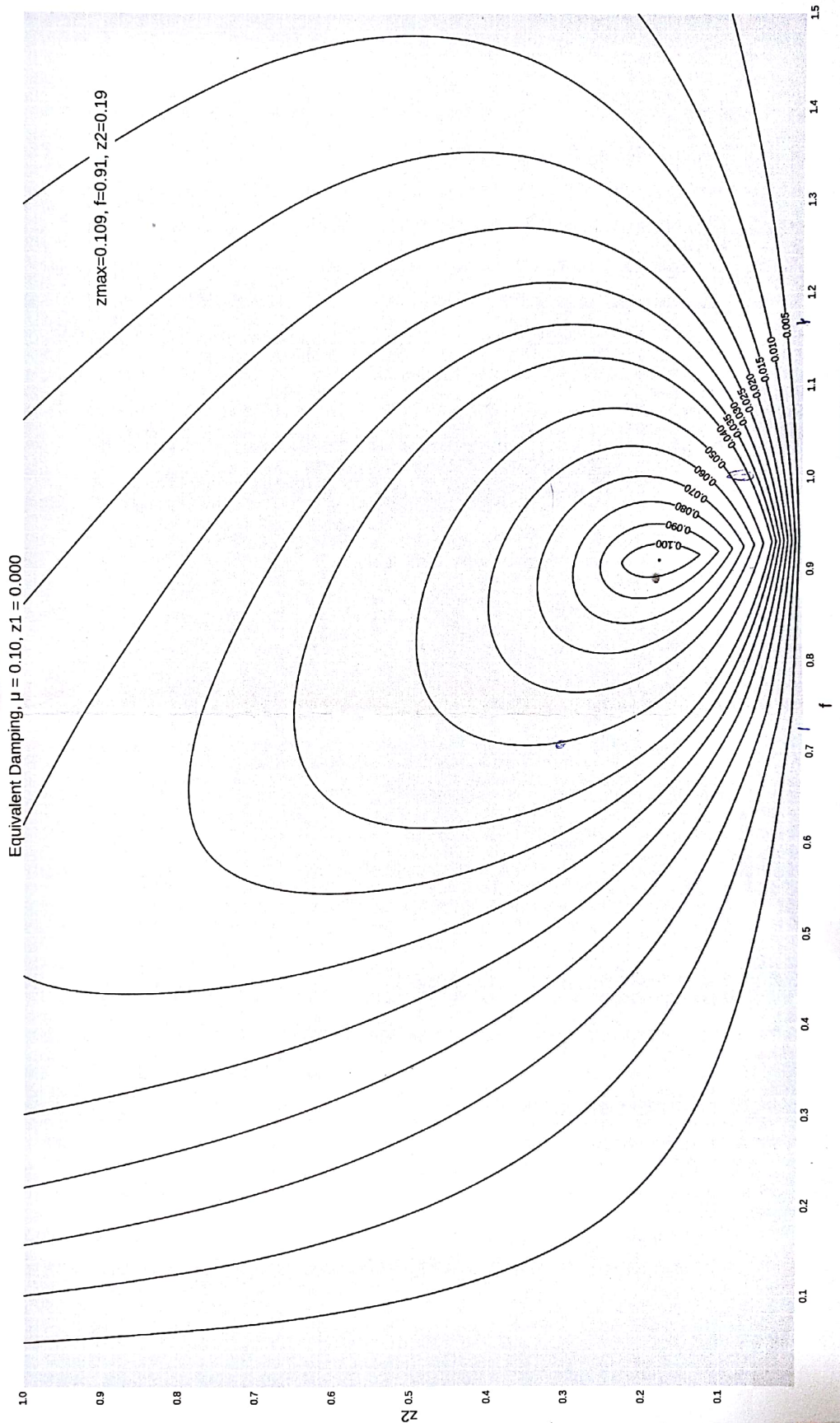


Figure 7.1: Line diagram for damping calculation when a TMD is added[14]. So called "Bierum circles" for $\mu = 0.10$ and $z_1 = 0.000$. Frequency ratio q on the horizontal axis and the damping coefficient on the vertical axis. Added damping is written on each line.

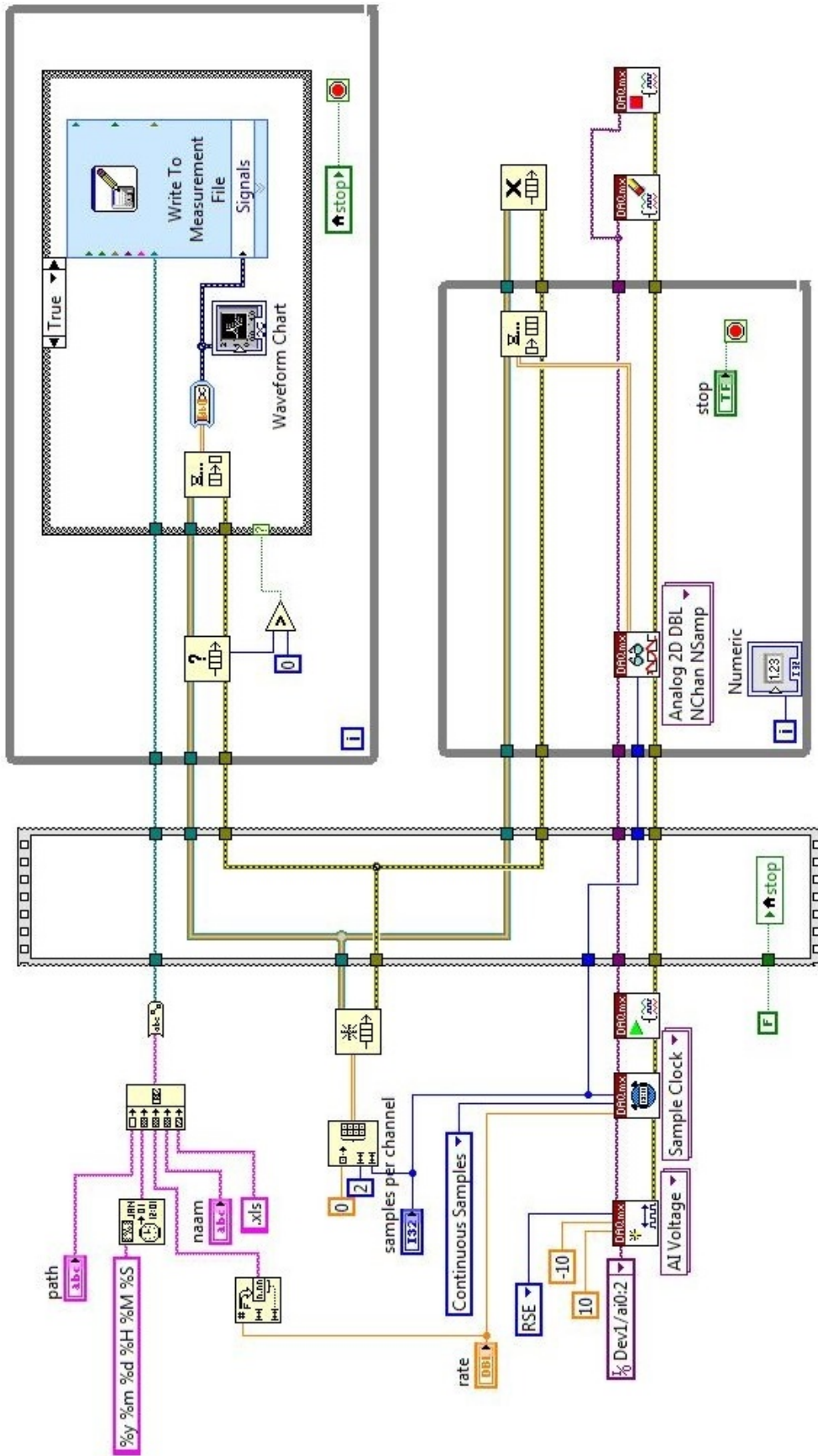


Figure 7.2: Block diagram that processes the data from the laser displacement sensor into Excel files.

Appendix C



Figure 7.3: SCARA system subjected to measurements.



Figure 7.4: Double balancing system subjected to measurements.

Functional Principle, Technical Data

3.3 Technical Data ILD 1402-x

Model	ILD	1402-5	1402-10	1402-20	1402-50	1402-100	1402-200	1402-250VT	1402-400	1402-600
Measuring range	mm	5	10	20	50	100	200	250	400	600
Start of range	mm	20	20	30	45	50	60	100	200	200
Midrange	mm	22,5	25	40	70	100	160	225	400	500
End of range	mm	25	30	50	95	150	260	350	600	800
Linearity	µm	5 ... 9	5 ... 18	7 ... 36	12 ... 90	20 ... 180	40 ... 360	50 ... 1200	120 ... 2000	120 ... 3000
		≤ 0.18 % FSO								
		≤ 0.5 % FSO								
Resolution	Averaged over 64 values, µm	0.6	1	2	5	10	13	32	80	80
	dynamic, µm	1 ... 3	2 ... 5	5 ... 10	6 ... 25	12 ... 50	13 ... 100	32 ... 300	80 ... 480	80 ... 600
	1.5 kHz	0.02 ... 0.05 % FSO								
	digital	14 bit								
Measurement rate, programmable		1.5 kHz; 1 kHz; 750 Hz; 375 Hz; 50 Hz								
Light source		Semiconductor laser 1 mW, 670 nm (red)								
Laser class		Class 2 (II) acc. to IEC 60825-1: 2007								
Spot diameter	SMR, µm	110	110	210	1100	1400	2300	5000	2.6 x 5 mm	2.6 x 5 mm
	MR, µm	380	650	530	110	130	2200	5000	2.6 x 5 mm	2.6 x 5 mm
	EMR, µm	650	1200	830	1100	1400	2100	5000	2.6 x 5 mm	2.6 x 5 mm
Protection class		IP 67								
Vibration		15 g / 10 Hz ... 1 kHz								
Shock		20 g / 10 Hz ... 1 kHz								
Weight (without cable)		15 g / 6 ms (DIN EN 60068-2-29)								
Temperature stability		approx. 83 g								
Operation temperature		0.03 % FSO/°C								
		0.08 % FSO/°C								
		approx. 130 g								
		0 ... 50 °C								

Figure 7.5: Device properties of the laser displacement sensor: ILD 1402-5.

Appendix E: m-file that calculates the system properties from the laser displacement data.

```
1 %S88 measurement calculations, 6/3/2017
2 clear variables; close all; clc;
3 %%
4 middle_directory = 'C:\Users\Niek\Documents\data\straight S88\middle';
5 x = load(fullfile(middle_directory, '17 03 02 08 37 05 1000smFlx-1x.xls'));
6 T = length(x)-0;
7
8 %raw data
9 x1 = x(1:T,1); %acc. x-direction
10 x2 = x(1:T,2); %acc. y-direction
11 x3 = x(1:T,3); %acc. z-direction
12 x4 = x(1:T,4); %displacement sensor
13
14 Fs =1000; %sampling frequency
15
16 %voltage to displacement
17 C_disp = 5/8.29; %[mm/V], sensor property
18 x4 = x4-1.9115;
19 x4 = x4*C_disp; %[mm]
20
21 L = length(x4); %signal length
22 t = linspace(0,L/1000,L);
23
24 figure(1);
25 plot(t,x4)
26 ylabel('Displacement [mm]'); xlabel('time [s]')
27
28 %% stiffness calculation
29 b1 = 1; e1 = 4500;
30 b2 = 5500; e2 = 8100;
31 b3 = 9300; e3 = 11700;
32 b4 = 12700; e4 = 14500;
33 b5 = 16400; e5 = 17800;
34 b6 = 20080; e6 = 21620;
35
36 d_norm = mean(x4(b1:e1));
37 d_200 = abs(d_norm - mean(x4(b2:e2)));
38 d_400 = abs(d_norm - mean(x4(b3:e3)));
39 d_600 = abs(d_norm - mean(x4(b4:e4)));
40 d_800 = abs(d_norm - mean(x4(b5:e5)));
41 d_1000 = abs(d_norm - mean(x4(b6:e6)));
42
43 dist = [d_200 d_400 d_600 d_800 d_1000]';
44 vhnd = mean(dist./(1000*[2 4 6 8 10]'));
45 kmean2 = 1/vhnd;
46
47 figure(3)
48 plot(x4)
49 hold on
50 linerange = [-0.1 5.1];
51 line([b1 b1],linerange,'Color',[1 0 0])
52 line([e1 e1],linerange,'Color',[1 0 0])
53 line([b2 b2],linerange,'Color',[.5 1 0])
54 line([e2 e2],linerange,'Color',[.5 1 0])
55 line([b3 b3],linerange,'Color',[1 1 0])
56 line([e3 e3],linerange,'Color',[1 1 0])
57 line([b4 b4],linerange,'Color',[1 0 1])
58 line([e4 e4],linerange,'Color',[1 0 1])
59 line([b5 b5],linerange,'Color',[0 0 1])
60 line([e5 e5],linerange,'Color',[0 0 1])
61 line([b6 b6],linerange,'Color',[0 0 0])
62 line([e6 e6],linerange,'Color',[0 0 0])
63
```

```

64 title('Full displacement data of the S88')
65 xlabel('t [s]'); ylabel('Displacement [mm]')
66 % k = [2 4 6]./([d_200 d_400 d_600]/1000);
67 k = [2 4 6 8 10]./(dist/1000);
68 kmean=mean(k(1:5));
69
70 %% normalize
71 y4 = x4(24941:end);
72 avg = mean(y4);
73 y4 = y4 - avg;
74
75 L = length(y4); %signal length
76 t = linspace(0,L/1000,L);
77 figure(1);
78 plot(t,y4)
79 title('Normalized oscillations of the S88')
80 xlabel('t [s]'); ylabel('Displacement [mm]')
81
82 %% FFT displacement
83 y1 = fft(y4);
84 P2 = abs(y1/L); % two-sided spectrum
85 P1 = P2(1:L/2+1); % single sided spectrum
86 P1(2:end-1) = 2*P1(2:end-1);
87
88 f = Fs*(0:(L/2))/L; % frequency domain
89
90 figure(2)
91 plot(f,P1)
92 title(sprintf('single-sided spectrum of S88, displacement'))
93 xlabel('f [Hz]');xlim([1 80]);ylabel('|P1(f)|')
94
95 hold on
96 index2 = find(P1 == max(P1));
97 index3 = f(index2);
98 line([index3 index3],[0 max(P1)/25],'Color',[1 0 0])
99
100 %% max amplitude fit
101 A = round(mean(find(y4 == max(y4))));
102 B = y4(A);
103 figure(1)
104 hold on
105 plot(0,B,'*')
106 zeta = 0.16;
107 omega_displ = index3;
108 fit = B*exp(-zeta*omega_displ*t);
109 fit2 = -1*B*exp(-zeta*omega_displ*t);
110 plot(t,fit,'r')
111 plot(t,fit2,'r')
112
113 disp('zeta = '); disp( zeta);
114 disp('omega_disp = '); disp(omega_displ);
115 disp('k = '); disp(k);
116 disp('k_mean = '); disp(kmean);
117 disp('compliance'); disp(1/kmean);

```

Bibliography

- [1] N.F. de Wit, *Support systems for surgical microscopes*, Literature survey, December 2016
- [2] <http://www.leica-microsystems.com/products/surgical-microscopes/ent/details/product/leica-m525-f50/>
- [3] Carr, Gary B., and Carlos AF Murgel. "The use of the operating microscope in endodontics." *Dental Clinics of North America* 54.2 (2010): 191-214.
- [4] Mungadi IA. Refinement on Surgical Technique: Role of Magnification. *Journal of Surgical Technique and Case Report*. 2010;2(1):1-2. doi:10.4103/2006-8808.63705.
- [5] Shuhaiber, Jeffrey H. "Augmented reality in surgery." *Archives of surgery* 139.2 (2004): 170-174.
- [6] Herder, J. L., et al. "Efficiently variable zero stiffness mechanisms." 4th International Workshop on Human-Friendly Robotics, The Netherlands. 2011.
- [7] Uluç, Kutluay, Gregory C. Kujoth, and Mustafa K. Bakaya. "Operating microscopes: past, present, and future." *Neurosurgical focus* 27.3 (2009): E4.
- [8] Jabbour, Pascal M. *Neurovascular Surgical Techniques*. JP Medical Ltd, 2013.
- [9] Metelski, Andreas. "Ceiling mount." U.S. Patent No. 6,364,268. 2 Apr. 2002.
- [10] Ludwig, Manfred. "Three-dimensional adjustable ceiling suspension for a surgical microscope." U.S. Patent No. 5,271,592. 21 Dec. 1993.
- [11] Kersten-Oertel, Marta, et al. "Augmented Reality for Specific Neurovascular Surgical Tasks." Workshop on Augmented Environments for Computer-Assisted Interventions. Springer International Publishing, 2015.
- [12] B. Bakker and J. van Seggelen, 2010, The revolutionary Hummingbird technology, *Mikroniek* 50 (2), pp. 14-20.
- [13] http://www.brown.edu/Departments/Engineering/Courses/En4/Notes/vibrations_free_undamped/vibrations_free_undamped.htm, visited: April 3, 2017
- [14] <https://flow-engineering.com/tuned-mass-dampers/>, visited: June 27, 2017
- [15] Den Hartog, J. P., and JP Den Hartog fourth edition *Mechanical Vibrations* McGraw-Hill Book Company, Inc., New York, 1956.
- [16] El-Hami, M., et al. "Design and fabrication of a new vibration-based electromechanical power generator." *Sensors and Actuators A: Physical* 92.1 (2001): 335-342.
- [17] Abubakar, I. M., and B. J. M. Farid. *Generalized Den Hartog tuned mass damper system for control of vibrations in structures*. London: WIT Press, 2013.
- [18] Howell, Larry L. *Compliant mechanisms* John Wiley & Sons, 2001.

FIGURES

- [19] <http://www.leica-microsystems.com>, visited: October 13, 2016
- [20] <http://www.laboamerica.com/products/dentistry/prima-dnt-trainer>, visited: October 17, 2016
- [21] <http://www.zeiss.com/meditec>, visited: October 13, 2016
- [22] http://www.medicalexpo.com/medical_manufacturer/ceiling-mounted-surgical-microscopy-29657, visited: October 17, 2016